UNIVERSITY OF CALIFORNIA
RIVERSIDE

Design, Fabrication, and Characterization of Optical and Magnetic Thin Films for Futuristic Nanotechnologies

A Dissertation submitted in partial satisfaction
of the requirements for the degree of

Doctor of Philosophy

in

Materials Science and Engineering

by

Brandon N. Davis

June 2019

Dissertation Committee:
Alexander Khitun, Chairperson
Nissim Amos
Suveen Mathaudhu

The Dissertation of Brandon N. Davis is approved:

_____

_____

_____

Committee Chairperson

University of California, Riverside

Acknowledgements

Throughout the process of obtaining my PhD, I received support from many different people before, during, and now upon the completion of this dissertation. My achievements would not have been possible without all their support and belief in me.

I would like to thank my dear family that saw me through this challenging endeavor. I feel fortunate that they have been there for me continuously and consistently, always helping me undertake new goals and believing in my ability to conquer them. Without their unwavering help, this achievement would have not been possible.

I thank the staff, administrators, and faculty at the University of California – Riverside Bourns College of Engineering and Graduate Division. Being given the opportunity to attend, learn, and thrive at this institution of higher learning has pushed me to new heights educationally and industrially.

I would like to thank my advisor, Nissim Amos, for guiding me through the path of truly understanding what it means to be a good researcher and goal-driven strategist. With his support, I am now able to undertake my post-graduation goals with full confidence.

I wish to also thank everyone who supported me whom I didn't mention here.

ABSTRACT OF THE DISSERTATION

Design, Fabrication, and Characterization of Optical and Magnetic Thin Films for Futuristic Nanotechnologies

by

Brandon N. Davis

Doctor of Philosophy, Graduate Program in Materials Science and Engineering
University of California, Riverside, June 2019
Dr. Alexander Khitun, Chairperson

With the continuous advancement of nanoscale-based data storage and memory technologies, a significant reduction in the dimensions of various materials and devices lead to an array of advancement-hindering phenomenon. The roadblock for these technologies is to find nanomaterials that can support the operation and progression with reducing scales. The focus of the presented research is to create new thin film compositions that take advantage of already optimized conventional materials. We explore layering different thin films in a way that uses the strength of each material while minimizes their weaknesses. These multilayer thin films are tailor-made to the specific functionality of a device or technology. In this work, design, fabrication, and characterization solutions relating to optical-based and magnetic-based futuristic nanotechnologies are explored.

Near field Scanning Optical Microscopy (NSOM) is a nondestructive optical characterization technique that allows for optical analysis beyond the diffraction limit. To further advance this nanophotonics technology, the fabrication and analysis of novel Al/Ag multilayers thin films is developed and optimized. Our research data shows that the proposed nanomaterial produces relatively smaller grain sizes, higher grain density, lower roughness, better uniformity and higher predictability while still exhibiting outstanding

optical properties. Results will be shown on how alternating grain sizes and grain boundaries between each of the Al and Ag bilayers is the main cause for such properties. Capable of enabling smaller and more uniform apertures with relatively less light "leakage, the newly developed compositions will be of major importance to the progression of broadband near-field scanning optical microscopy.

The exploding need for higher density storage devices recently led to innovative solutions to further increase the capacity of conventional Hard-disk Drives. One such technological solution is 3D-Multilevel magnetic media with microwave-assisted data recording. Continuing with the application of advanced optics and the multilayers approach, the goal for this research is to develop Co/Pd Mulilayers thin film, which have at least two magnetic recording layers that are both magnetically and electrically decoupled. To effectively analyze such media, much investigation went into custom-designing and assembling a nondestructive and scientifically credible optics-based magnetometery system. Results for this system, which is based on the Faraday Effect, reveal its capabilities of producing data for each recording layer across the thickness of 3D Multilayers Co/Pd media. The design consideration, fabrication, and analysis data for such media using SiO_2 as a decoupling, seed, and capping layer along with in-situ applied magnetic field will be presented. The Faraday Effect-based system further proved effective in analyzing the magnetic properties of Yttrium Iron Garnet (YIG) structures. As is well known, YIG is a candidate material for the advancement of spintronics, a field that can greatly expand the functionality of current semiconductor memory technologies. Magnetic properties data is presented for both uniform YIG-based thin films and patterned structures.

Table of Contents

Contents

List of Figures

List of Tables

Introduction

The Continuous Scaling of Data Storage and Memory Technologies

Gordon Moore noted that the number of transistors per square inch on transistors doubled approximately every 18 to 24 months, an observation that eventually became known as "Moore's Law" [1]. The observation of Moore's Law has led to the development of a semiconductor roadmap for different technologies and devices within the industry [2]-[3]. This roadmap has guided the continuous advancement of the data storage and semiconductor industries and has resulted in both the scaling down of device dimensions and the scaling up of the computing capacity and number of transistors [3]. Fundamentally, smaller devices for both semiconductor and data storage applications result in more devices per unit area and a higher memory and data storage per system, respectively. The design rules for these devices must account for Dennard Scaling principles that outline different aspects of the devices that may be affected due to scaling-down [4]. Currently, the many laws dictating design rules are approaching different physical limits, which will result in new phenomenon at sub-10-nm sizes that are not fully understood. Hence, extensive resources and efforts have been expended in material-centric research to design and manipulate conventional materials to break through these limits [5].

This dissertation will explore potential solutions for some of these issues in the fields of magnetic and optical-based data storage and semiconducting devices. The issues that arise in these materials are based on separate phenomena that occur because of the continual scaling down in the size of their related technologies. There are many novel materials being developed to address these phenomena, but many are still at the research phase and many years may pass before they reach commercial viability [4]. Thermal limitations in magnetic materials in hard disk drives are one of

the fundamental restrictions in higher-density storage. Due to the superparamagnetic limit (as magnetic media grains dimensions scale down), the magnetic poles within a material that reaches this limit will start flipping randomly due to temperature instability [6]. Thus, since the magnetic poles define binary storage, magnetic-based data stored in hard-disk drives becomes unstable and unusable.

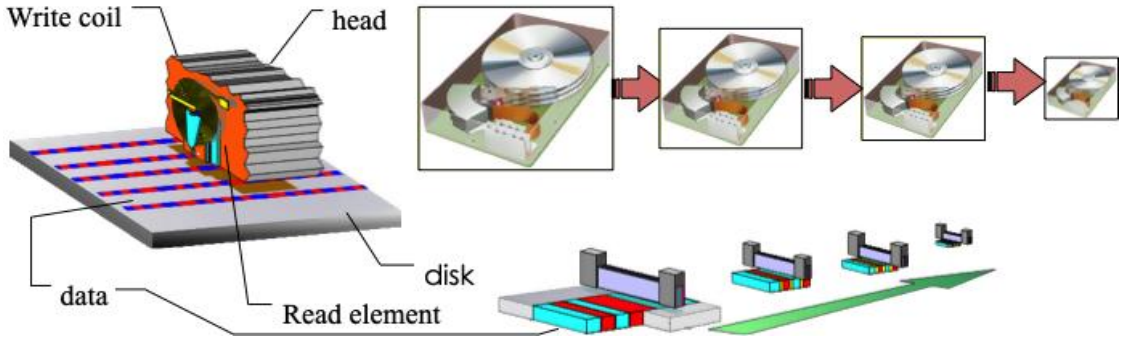

Figure 1 An image illustrating the continuous scaling down of the hard disk drive.

In terms of optical-based characterization and analysis, as these devices further scale below the diffraction limit, a critical need arises for nano-optics materials that can maintain the integrity of their fundamental optical properties [7]. The limit of functionality in general (depending on the light source used) is ~ 200 nm within the standard dimension of the material. Below this size, new and challenging phenomena are encountered with various optical materials that limit the functionally of devices with decreasing scales [8]. In other words, while bulk materials and thin films with relatively large thicknesses are both understood and work well for various existing applications, as the scale of data storage and semiconducting technologies continuously decrease, a variety of critical properties change adversely. Nevertheless, there are some circumstances for which not all properties of magnetic or optical thin films degrade under reduced thicknesses and device dimensions. This observation leads to the focus of this dissertation which is to find solutions to selected open questions relating to current scaling-related technological challenges.

This presented research explores the layering of materials in multiple stacks to take advantage of specific materials properties to overcome another material's shortcomings. Multilayer (ML) media has proven to be highly effective in this respect, and it has allowed materials to reach sub-25 nm size scales with a 2:1 thickness ratio between layers. It was expected to create a novel material stack that addresses material property issues on a continuously decreasing scale.

The Need for Alternate Technologies

Applications and Limitations of Near-field Scanning Optical Microscopy

The first question to be answered in this thesis is whether it is practically possible to innovate near-field scanning optical microscopy (NSOM) probes with spatial resolution enhancements, along with broadband light analysis capabilities. NSOM is a powerful optical technique that operates beyond the diffraction limit within the optical near-field zone. This microscopy technique enables optical imaging that has a resolution that is potentially an order of magnitude better than conventional optical microscopes. Furthermore, since the technology is embedded on an atomic force microcopy system, both 3-dimentional (3D) morphology with sub-nanometer resolution and optical properties are gathered simultaneously. Among other applications, NSOM is important to the development of near-field transducers for so-called heat-assisted magnetic recording technology, which is predicted to extend the areal density limitation of conventional technology. With respect to biology-related advancements, it allows individual molecules and cells to be optically analyzed, as shown in Figure 2b.

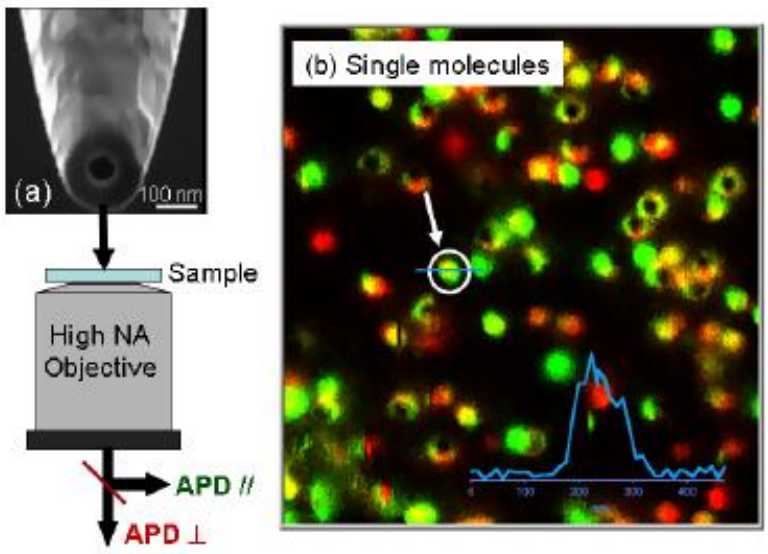

Figure 2a) SEM images of an NSOM tip encased in the aperture material along with the imaging technique used to collect the near-field light as it exits the sample; b) An NSOM image revealing the optical properties of a single molecule [9].

A standard NSOM tip is composed of a fiber optic wire encased in a metallic aperture [10]–[12]. Two of its primary limitations are light "leakage" through the granular sidewalls of the aperture and a limited optical broadband range which are mainly due to the materials typically used [10]. Currently, the most popular material is single-layer aluminum because of its excellent optical properties, specifically its reflectivity of broadband light. Nevertheless, the use of aluminum thin films is limited by their surface roughness, large grain boundaries, and oxidation [10], [11].

Research in this area involves the development and analysis of unique multilayer (ML)-based thin films using aluminum (Al) and silver (Ag). Unlike previous attempts to produce Al/Ag-based alloys, the focus here is on multilayered structures of laminated Al/Ag bilayers. Since this method allows each material to retain its distinctive properties, the result is the superposition of both material properties in a single thin film. For example, one goal of the current research was to determine if it was possible to combine the optical and electrical properties of both Al and Ag to obtain exceptional microstructures (surface, grain size, and grain boundaries) in a single thin film.

Applications and Developments of Spintronics

As challenging limitations draw closer for higher integration and down-sizing of transistors for processing applications, alternate technologies are being developed to create faster, more energy efficient, and more powerful proficient central processing units. Spintronics is one example of these new technologies which uses the spin-nature of electrons to process information, which is different from conventional technology were a single binary digit is stored or processed with a quantity of charges. Yttrium iron garnet is an intensely-studied candidate material for the advancement of spintronics, a field that has the potential to greatly expand the functionality of current semiconductor complementary metal-oxide semiconductor (CMOS) technologies [13]. The figure below shows a proposed spintronics-based device and its information processing method [14].

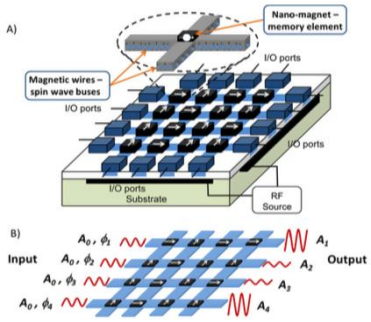

Figure 3 A) Proposed design for a magnonic-based holographic memory (MHM) device; B) Illustration of the operation of the device

The proposed device underwent extensive magneto-electrical characterization to demonstrate its concept and viability. Nevertheless, the magnetic properties of the YIG thin film and patterned device were still unknown. Research was devoted to determining if Faraday Effect Microscopy and/or Magnetic Force Microscopy were effective techniques to characterize YIG-based thin films and structures.

Current Developments and Limitations of Magnetic Data Storage

The recent rapidly expanding need for higher density storage devices has led to innovative solutions for further increasing the capacity of conventional hard-disk drives. Over the past two decades, perpendicular magnetic recording (PMR) technology has been slowly optimized to overcome the superparamagnetic limitation of its predecessor, longitudinal magnetic recording (LMR) technology. The predicted areal density of PMR technology is ~ 1 Tbits/in^2. Thus, more than ever before, the data storage industry is currently faced with technological challenges to propose and successfully manufacture alternate technologies that will continue the progression of higher areal density magnetic storage devices beyond 1 Tbits/in^2. One such solution is the use of 3D-multilevel magnetic media with microwave-assisted data recording [15]. The continued application of advanced optics and the multilayering approach for nanophotonic applications led to the goal of this research to develop Co/Pd multilayer thin films that at least two magnetic recording layers, which are both magnetically and electrically decoupled. To effectively analyze such media, significant efforts were made to custom-design and develop a nondestructive and scientifically credible optics-based magnetometry system.

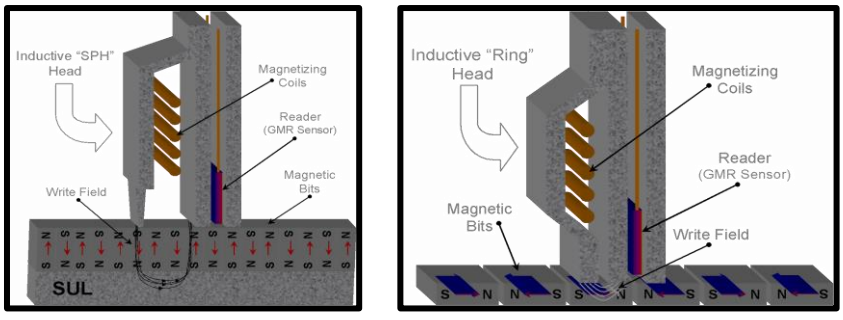

Figure 4 Conventional memory recording mechanisms: (left) former Longitudinal Magnetic Recording (LMR) and (right) present Perpendicular Magnetic Recording (PMR).

Conventional perpendicular magnetic recording media requires the magnetic materials to have a specific crystal structure to orient the magnetization in the out-of-plane direction [16]. To obtain this crystalline structure, several fabrication processes are needed to first properly deposit seed layers that establish the media grain size and boundaries [17]. Magnetic media may then be deposited using different deposition conditions and/or temperatures to create perpendicular magnetic recording (PMR) media [18]. The research here will focus on design, fabrication, and cauterization of Co/Pd multilayered PMR media for 3D ML microwave assisted magnetic recording (MAMR) applications. Magnetic media fabricated in this way possess a major advantage over present PMR media because the properties of each layer is independent from the previous layer's crystal structure. The perpendicular anisotropy is a result of the interface between the Co and Pd layers and the surface smoothness of the previous layer. Furthermore, independent magnetic recording layers (MRLs) can be produced by simply increasing the thickness of a Pd layer between the MRLs or by depositing other nonmagnetic materials as decoupling layers. While extensive research has been published on this type of media involving nonmagnetic and electrically-conducting separation layers [19], very little research has been devoted to investigating nonmagnetic and electrically-insulating decoupling layers [20]. The goal of this work is to investigate the potential of using SiO_2 as a separation, seed, and capping layers for the fabrication of 3D-ML MAMR media. Thus, it is necessary to maintain proper surface properties of the insulating layer so that the magnetic layer above it will also have perpendicular anisotropy.

It is well-documented that magnetic materials exhibit a preferred direction for magnetic moments, which is denoted as the easy-axis (EA) of magnetization. For most crystalline thin films, this is induced along a preferred crystalline direction. For example, most conventional hard disk drives (HDDs) use magnetic thin films to store binary information in the form of magnetic alignment of nanograins on the disk surface. The (EA) of such recording media is aligned in the out-of-plane

direction (perpendicular to the disk surface). This magnetization alignment is achieved by creating crystalline seed layers that induce the cobalt c-axis (hcp cell) of a magnetic material to point along the perpendicular direction. If a magnetic field is applied in the in-plane direction with increasing magnitude, the magnetization will eventually align along the direction of the applied field in the presence of an external field. Considering this, the alignment along this direction is possible only with a relatively greater magnitude than is required to switch the magnetization along the perpendicular direction. This alignment causes the magnetization to align along the hard-axis (HA) of the media. Thus, while an out-of-plane (along the EA) applied magnetic field will cause the magnetic domains within the material to permanently switch, an applied magnetic field in the in-plane direction (along the HA) will only temporarily rotate the magnetization. Once turned off, the domains will randomize. The question that this research attempts to address is whether application of an in-plane magnetic field during the deposition of Co/Pd ML magnetic recording media will affect its magnetic properties.

General Fabrication Techniques

The fabrication and characterization techniques described in this chapter were used to create the devices in this dissertation. The experiments were conducted at the University of California Riverside in the following facilities: The Center for Nanoscale Science and Engineer (CNSE), the Analytical Chemistry Instrumentation Facility (ACIF), and the Central Facility for Advanced Microscopy and Microanalysis (CFAMM). These are general use facilities maintained by staff that oversees equipment training, certification, and maintenance for independent operation.

Fabrication and Characterization

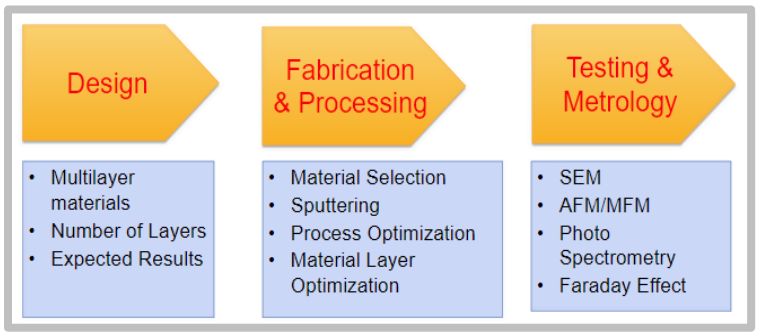

Figure 5 Materials fabrication process flow used to design experiments throughout this dissertation. This methodology separates the key techniques for successful implementation of design rules

A fabrication process flow was created involving a variety of techniques at different phases. The creation of ML media was designed top-down and then built bottom-up, and the parameters for each step were characterized to ensure the ideal setting for each process step to achieve the correct design criteria.

Photolithography

Ultraviolet (UV)-based photolithography is a process used to transfer a pattern onto a substrate and is the underlying technology for the entire semiconductor industry. The photolithographic process involves several steps that are focused around five main processes: photoresist application, post-apply bake, exposure, post-exposure bake, and development. Each process step must be optimized to ensure the pattern transfer onto the substrate results in the highest resolution.

Photoresists are sorted into two broad categories: positive- and negative-tone resists. The standard photoresists used are Shipley S1813 and AZ 5214, both positive-tone resists which are spin-coated to a designated thickness and post-apply baked to remove residual casting solvents. The parameters for these steps can be found in manuals, but they must be optimized for use in the facility. Exposure is performed using a Karl Suss MA6 mask aligner, which consists of two main channels that emit

different wavelengths exposure light. The i-line channel emits a wavelength of 365 nm at 5.5 mW/cm^2, and h-line emits a wavelength of 405 nm at 24 mW/cm^2. Both can be used for exposure, but the i-line is preferred due to less dispersion and lower line edge roughness. The exposure time is decided based on the thickness of the resist and thus the penetration depth of the light. The final step is photoresist development in a solution that dissolves the exposed parts, the lithography process is followed by an etch or deposition step of the photoresist. An etch step is then performed to transfer the lithographic relief pattern to the substrate.

A characterization process was developed to standardize a recipe using a photomask with a variety of feature sizes using a silicon wafer as the substrate. A standard process was developed to accommodate multiple feature sizes and different sample exposure times. The optimal development time was determined by developing the photoresist in 5-second increments, and development quality was visually confirmed with an optical microscope.

Figure 6 The Karl Suss MA6 mask aligner instrument used in the CNSE at UCR used to create patterned substrates.

Sputtering

Sputtering is a physical vapor deposition (PVD) process used to create a variety of thin film materials that uses gaseous Argon ions to create plasma, which is then accelerated at a target material. The target holder has an opposite charge from the ions which causes them to be accelerated toward it, dislodging parts of the material, which then coat a substrate that is above the target. This technique was developed as vacuum technologies advanced, resulting in more precisely controlled and uniform deposition rate at lower pressures and higher voltages.

Figure 7 The AJA sputtering system used to deposit many types of thin films. The system is capable of depositing multiple materials concurrently through either manual operation or automatic programming.

There are three main types of sputtering arrangements used in this dissertation: direct current (DC), radio frequency RF, and enhanced magnetron. Each type is specialized for use with specific materials. DC sputtering is mainly used for metals since metals are conducting which causes a negative bias on the target material that attracts the charged Ar ions. RF sputtering was implemented for both metals and oxides, though it is mostly essential for oxides. Applying an RF frequency creates both a negative and positive bias at the MHz range. Since an RF voltage cycles

between the two polarities it provides a path for the charges that accumulated on the surface of the target to dissipate and thus allow for sputtering to occur from dielectric targets. Enhanced magnetron sputtering is specifically applied to magnetic materials because it allows them to directionally and uniformly migrate from the charged target through the plasma onto the substrate. The sputtered material is characterized using two substrates: one patterned and the other plain.

Atomic Force Microscopy

Scanning probe microscopy (SPM) is a common technique used to understand surface properties of a material where a probe is moved laterally across a surface, generating a variety of data about the surface. The difference between each type of data generated using SPM is the way in which the probe is monitored as it moves across the surface. The form that is used in this dissertation is atomic force microscopy (AFM) where a probe tip is attached to a cantilever that scans across a sample's surface. The advantage to using this method is that AFM can be easily modified to measure a variety of surface properties at the nanoscale. The specific properties to be studied using AFM are surface topography and the magnetic forces.

Figure 8 Atomic Force Microscope (AFM) system used for MFM and AFM measurements. This system is capable of measuring surface roughness, thicknesses, and magnetic domains of the thin films.

The AFM systems used in this research were VEECO Dimension 3100 and 5000. Both were mounted on vibration isolation tables, which the 5000 model was also enclosed in an acoustic-shield chamber. There primary functions were to characterize the surface topography and the magnetic domain of thin films. The surface topography was characterized using the tapping mode which provides high-definition topography information and is capable of deciphering grain boundaries. The limiting factors are the tip fidelity and sharpness since a sharper tip has a smaller diameter which can scan the surface in a higher resolution.

The secondary mode is magnetic force microscopy (MFM) which uses a magnetic tip to scan across a magnetic surface to map out its magnetic domain distribution. To perform an MFM scan, the tip must be lifted above the surface to prevent direct contact during the scan. The tip is charged with a magnetic field and is scanned just above the surface, and the data is generated when the tip is attracted or repelled from above the surface based on the field in the specified area. A map is generated along a surface topography scan for comparison of the area of interest.

Scanning Electron Microscopy

Scanning electron microscopy (SEM) is an electron microscopy technique that generates 2D images of material surfaces. Electrons are accelerated towards and impact the surface of a material. As the electrons hit the surface, various signals are emitted from the area of impact and among which are secondary electrons. These electrons are then collected by a secondary electrons (SE) detector, which convert the quantity of electrons from each exposed location to a voltage which is then noted at a grayscale colored pixel on a computer screen. The factors for imaging samples in this work were the aperture size and scan mode.

Figure 9 Nova NanoSEM 450 scanning electron microscope used for high-resolution SEM imaging

The Central Facility for Advanced Microscopy and Microanalysis (CFAMM) has a Nova NanoSEM 450, for use within the facilities. The settings used to optimize the samples were based on the following: detector, aperture, final lens, spot size, and electrons scanned. The objective is to obtain ultra-high-resolution 2D images of surface topography and grain structures. The detector used for the experiment is the through-lens detector (TLD) which specializes in capturing SEs to generate images. Using this detector, the final immersion lens was chosen to obtain high-definition images. This lens mode places the sample close to the lens so that a spot size of 3.5 nm can be used for the scans. The voltage of the electron gun was then lowered from the standard 20 kV to 10 kV, since charging can prevent proper images from being obtained at higher voltages. The aperture lens selected was 30 μm, since this allowed the spot size to be further reduced to create a more stable beam and higher-resolution at a lower kV.

Spectrophotometer

The Analytical Chemistry Instrumentation Facility (ACIF) houses a Jasco J-815 circular dichroism (CD) spectrophotometer with a scan range of 180 nm – 1100 nm that is used to measure the transmittance, absorbance, and reflectance of samples. This technique allows the optical properties of a thin film to be understood in terms of transmittance and reflectance. The instrument is comprised of two main detectors, a spectrometer, and a photometer. The spectrometer produces desired wavelengths of light. A collimator transmits a beam from the light source into a monochromatic prism that splits the beam into a spectrum of wavelengths, and then a slit isolates each wavelength so that only the desired wavelengths are emitted. A photometer measures the total remaining photons after the desired property is measured, and each property is measured based on the variety of stages and positioning of the detector. For reflectance, a sample is placed on a stage that has a small opening for the photons to be emitted, and light is reflected into an opening at an angle into the detector. A transmitter is placed in between the holder and detector, photons are emitted, and the detector reads the total percentage that penetrates the sample.

Figure 10 CD spectrophotometer used for the optical analysis of Al and Ag thin films

Magneto-Optic Kerr Effect

The magneto-optic Kerr effect (MOKE) is used to measure the magnetic hysteresis of a material where polarized light is transmitted through a sample that is magnetized using an electromagnet. When the light interacts with a magnetized sample the polarization angle of the resulting transmitted light changes. This light is then reflected through the dielectric layer in response to a magnetic field. These phenomena represent the Kerr and Faraday effects, respectively. The detector measures this Kerr signal and generates a hysteresis plot, and the system can measure the Kerr signal in three main modes: polar, longitudinal, transversal, and transmission mode. The transition mode is also known as the Faraday Effect mode. Each mode is used based on the type of magnetic media applied to the material.

Figure 11 The system set up used in transmission mode (Faraday Effect).

Figure 11 outlines the standard set up for the system in transmission mode which consists of several main components that include: a monochromatic laser, electromagnet, post-elastic modulator (PEM), lock-in amplifier, and detector. The monochromatic laser produces a beam of ~ 630 nm

wavelength which travels through a lens, which focuses the light prior to entering the electromagnet. The lock-in amplifier is tuned to the specified 2f signal of the modulated light beam prior to loading the sample and applying the magnetic field. This normalized the system to minimize noise and signal offsets before the experiment. The sample stage is placed on almost equal distance between both magnetic poles, and the field is applied incrementally +/- tesla. The laser passes through the PEM that modulates the signal at a constant rate of 50 kHz to stabilize the signal, which allows for a fast measurement with high accuracy. The detector reads changes in the linearly polarized light beam as the applied magnetic field changes, which generates the hysteresis curve.

Novel Coating for NSOM Probes to Enable Higher Resolution and Broader Optical Spectrum Analysis of Nanolasers

Attempts at optical imaging beyond the limits of human vision began with the invention of the optical microscope. This breakthrough ushered in the era of nano-optics which allowed humans to perceive things beyond the limit of our eyesight, when the first biological cells were imaged [14]. The understanding that objects exist beyond the basic human senses led to a desire to create devices that pushed past natural limitations to begin to understand how the world operates at smaller scales. Light, which is composed of photons, is both an electromagnetic wave and a particle that eyes use to decipher and then create images [15]. Due to the ever-decreasing scale of devices and technology, fundamental limitations have made it difficult to use standard light-based optical imaging techniques, and it is essential to develop technologies that can create higher-quality images at smaller scales.

Light is fundamentally perceived in far-field and near-field zones, which are regions where electromagnetic fields scatter around an object. This is what optical devices and materials interact with and manipulate [16]. The far-field, referred to as the Fraunhofer diffraction zone, occurs at farther distances from the scattering object, and light is primarily composed of these waves [17]. Far-field has been the typical field that we operate with, and it is composed of electromagnetic fields with many electric dipoles. The far-field carries uniform waves over longer distances, which allows for stable waves that enter an infinite distance and is the basis of telecommunication technologies [18]. Near-field, also known as Fresnel diffraction, occurs in the range closer to the scattering object. The near-field is split between the non-radiative zone and the radiative zone, and these zones are composed of multi-pole fields with a phase relationship [19]. This can cause

interference and noise once this zone is entered due to the many non-uniform interactions occurring between various poles [20]. Based on the understanding of the Fraunhofer and Fresnel theories, it is known that diffraction is the limiting factor for further advancements in optical microscopy.

Sub-diffraction Limit Microscopy Using NSOM

There is a growing need to characterize and understand high-density data storage devices as well as other applications that need high resolution images using visible light [21], [22]. With the continual scaling into the nanometer range, modern technologies developed beyond the diffraction limit of conventional optical microscopy. Whenever an object is imaged by an optical system, lens features smaller than half a wavelength of light are lost, as determined by Abbe in 1873 [23]. There have been many attempts to break this limit using super-lenses, lasers, and fluorescence microscopy [23]-[25]. Biological applications, for example, need to overcome this limitation to map out single molecules and cells in 3D to better understand their morphologies [26].

In standard confocal microscopy, light is transmitted by a monochromatic light beam which is then transmitted, reflected, or scattered by an object in a characteristic way that is collected by a lens and imaged onto a detector. For practical reasons, the lens is placed at least several wavelengths, λ, of illuminating light away from the object surface in the far field [27]. At these spatial frequencies, object details can be generated which then decay as the space decreases between the lens and the sample. The diffraction limit is defined as: $\Delta x = \lambda 2\pi NA$ where NA is the numerical aperture, which is between 1.4-1.6 in modern optics, and the standard λ of green light is 500 nm. Using these values confirms that the limit for confocal microscopy is 200 - 300 nm [28]. For the level of resolution that is needed for modern day technology, this resolution is not enough since modern optical microscopy needs information in the near-field range.

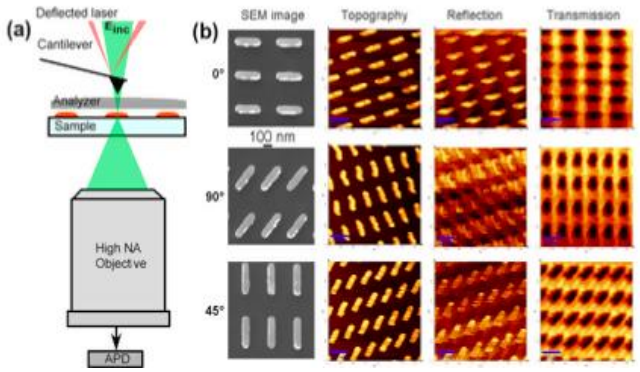

Figure 12 a) Diagram of the NSOM apparatus; b) An example of the NSOM application. Specifically, a sample is placed under the analyzer with the light coming from the tip, and the objective is placed under the sample [9].

NSOM was first proposed by Synge in 1928 as way to use an aperture capable of analyzing surface images smaller than the wavelength of light [29]. The properties of apertures are not are able to break through the diffraction limit, which limits optical imaging to ~ 200 nm. The optical near-field region is defined by approximately $\lambda/2$, where λ is the wavelength of light as defined by the Rayleigh criterion [30]. As can be seen in Figure 13, this optical scanning method is comparable to SEM, but the advantage of this method is its non-destructive nature, which other imaging methods can cause. The basic components of NSOM include the objective, light source, the tip, and the sample being analyzed [31]. There are different mechanisms to exploit this, but the method using a metal-coated AFM tip is of most interest. This mechanism works similarly to AFM, and it scans near the surface using a laser on the end of the cantilever to measure force feedback on a detector screen. It is also possible to fabricate a tip from a fiber optical wire that has been tapered and coated with a metal aperture [32]. This scanning method is slower but offers images with the highest resolution when compared to optical microscope images, as seen in Figure 13.

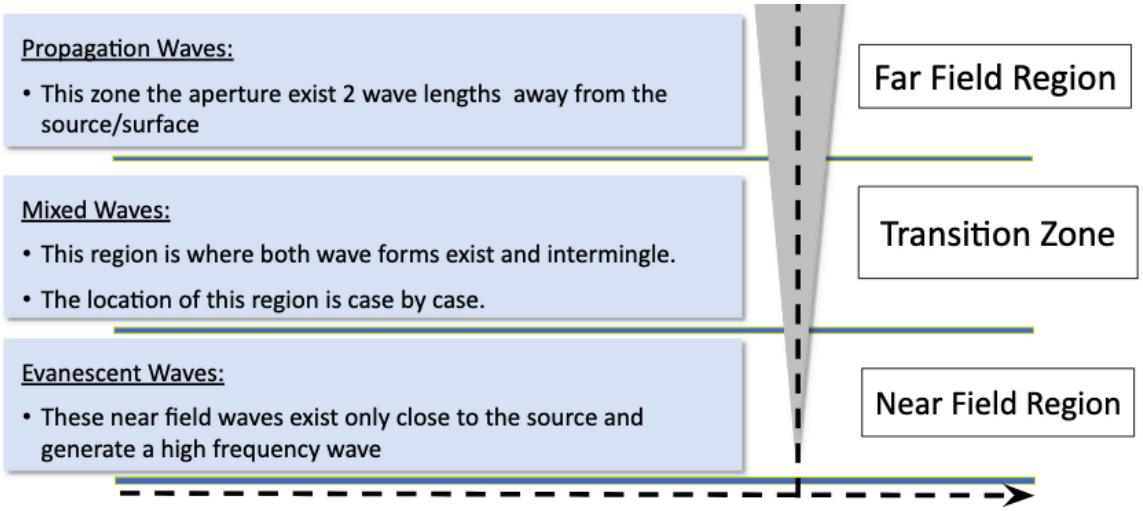

Figure 13 Description of the operating regions of different waves in Near Field and Far Field regions

NSOM is a 2D optical technique using broadband light wavelengths that is like confocal optical microscopy, but it operates in the near field region. As shown in Figure 14, NSOM zones are divided into the near-field region, transition zone, and far-field region, and different waves propagate in each region. NSOM attempts to operate in the near-field region by analyzing evanescent waves that exist closest to the surface. Evanescent waves interact with fine features in the sample being analyzed to provide the highest resolution images possible. These waves dissipate as they move to the transition zone, and because of this, the probe must remain in the near-field zone. The AFM feedback mechanism is excellent at maintaining a constant distance between the sample and probe. This special characteristic of AFM-based NSOM is due to the laser tip force feedback mechanism in the tip which can be accurately maintained in the sub-wavelength zone [33], [34].

The operation modes for a standard NSOM system are shown in Figure 14, which shows the location of the evanescent wave with respect to the sample as well as the wave propagation direction with respect to the laser source and sample. In this image, there are two focus modes that directly

relate to this research, including the apertureless method and the aperture method [35]. The aperture is composed of a fiber optic cable that is tapered or in the cantilever-based design as a hollow SiO_2 pyramid, and the fabrication of this is described in previously-published results [36]-[39]. Apertureless scanning probes have proven effective for near-field imaging, but the quality of the images is affected by scattering, confinement, and field enhancement characteristics [40]-[44]. However, to achieve ultrahigh-resolution imaging with relatively low background noise using these scanning modes, an aperture must be added to the tip [20].

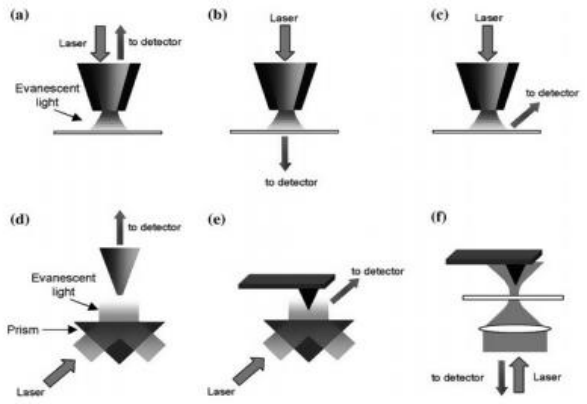

Figure 14 NSOM operation modes: a) illumination, b) collection, c) illumination collection, d) reflection, e) transmission collection and ,f) reflection collection [35]

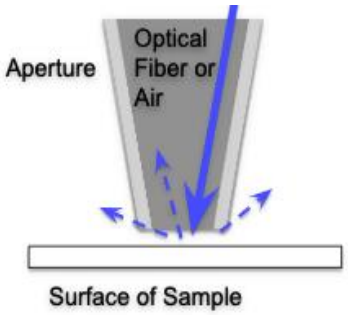

Figure 15 The components of the NSOM aperture and the interaction of light with the sample in near-field.

The aperture is a metallic material that encases the fiber optic wire which confines light that enters the tip. In the case of cantilever-based probes, a transparent hollow tip is coated with the metallic material. This causes the evanescent light waves to be retained within the optical tip, which keeps waves from escaping and prevents scattering from far-field waves as they travel along the fiber optic probe and towards the aperture [45]. After the fiber tip has been fabricated, an aperture is then processed by evaporating aluminum onto the sides of the fiber taper surface [46]. The result is an aperture with a diameter around 80-100 nm, which comes with additional issues [47], [48]. On the other hand, the cantilever based probes are sputter-coated with aluminum completely, following which an aperture is milled at the apex of the tip using a focused ion beam (FIB) system. Apertures with dimension below 50 nm are doable with this method. While NSOM probes are excellent at improving resolution, the normal material used in them is aluminum which has many defects from the processing which affects material properties at the nanoscale [49].

One of the challenges for physically evaporated aluminum coating is its grainy structure. For NSOM probes this includes the grains at the very end of the probe which decrease the overall optical imaging capabilities [50]. The grains increase the distance between the aperture and the sample which leads to a reduction in both resolution and intensity. The near-field confinement of the light emerging the probe is lost with increasing distance, and the intensity decays exponentially [51]. Further drawback of aluminum thin films are their relatively large grain boundaries, through which light "leaks" at the apex of the NSOM tip and thus further degrading its capabilities. Alternative materials include gold and silver, and as shown in Figure 16, these materials do not perform like aluminum across the entire broadband light range. Furthermore, gold has poor adhesive properties which can degrade the aperture over time. Comparing the materials in Table 1 shows that no material is capable of being used in a standalone application.

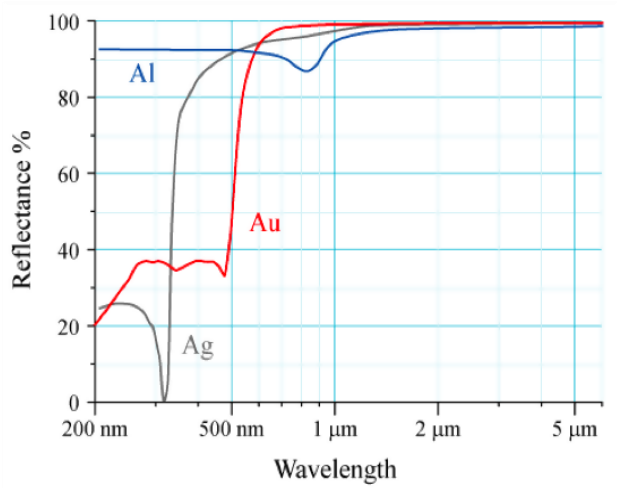

Figure 16 Typical reflectance optical spectroscopy for Al, Au, and Ag

[35] Material	Adhesion	Optical	Surface	Electrical	Cost	Deposition
Gold (Au)	Poor	Good	Excellent	Excellent	High	Limited
Silver (Ag)	Excellent	Good	Excellent	Good	Medium	Variety
Aluminum (Al)	Excellent	Excellent	Poor	Excellent	Low	Variety

Table 1 Relative rating of each material key characteristics for optical applications

Proposed Solution

As mentioned before NSOM is a nondestructive optical characterization technique that allows optical analysis to be performed beyond the diffraction limit. Over the last few decades (patented by Pohl in 1986), this method has been extensively studied and has shown to be highly effective at creating high-resolution images beyond the diffraction limit. The basic components for NSOM include an objective, a light source, a tip with an aperture, and the sample being analyzed [9][26].

A key component is the aperture, this enhances the ability of the NSOM tip to confine evanescent light waves which minimizes the number of waves that escape and reduces scattering from far-field waves as they travel along the fiber optic probe. After fabrication of the tip, an aperture is processed using physical vapor deposition (PVD) to deposit a material onto sides of the tip surface [46][47]. While the addition of an aluminum aperture significantly improves NSOM functionality, there are still limitations to the surface and optical properties that ultimately degrade the quality of the resulting images [34][44]. As illustrated above, aluminum thin films exhibit a grainy structure, which allows light to escape through the larger interfaces as it propagates along the probe. Additionally, the grains increase the distance between the aperture and the sample which leads to a reduction in both resolution and intensity: the near-field confinement of the light emerging from the probe is lost with increasing distance, and the intensity decays exponentially [4][5][32][39][40]. There have been a variety of materials used individually for improvement in limited broadband light wavelengths because of optical and surface properties limiting their effectiveness [41][42]. Nevertheless, the main benefit for aluminum exhibiting an overall great optical reflectance properties for a large broadband of light and hence at this time is the material of choice for commercially available NSOM probes.

When developing an improvement for the aperture it is important to understand current materials that have been implemented also are limited based on two mechanisms of reflection, which are specular reflection and diffuse reflection. Both phenomena influence metallic thin film materials. Specular reflection is the classic reflection mechanism, where the incident light interacts with metallic material creating a mirror image. When interacting with metallic surfaces the electrons begin to oscillate, this creates a radiating field that does two things: 1) cancels the incident light and 2) generates a backward radiating field that reflects the incident light. Diffuse reflection, on

the other hand, occurs when light interacts with crystalline materials that contain grains and thus grain boundaries. The gaps between grains result in a variety of angles that are dissimilar to the incident beam of light, causing it to scatter in all directions. However, some light can still penetrate at time through the grain boundaries. By taking these two factors into the design we determined that no one material can perform optimally throughout the entire spectrum of light.

This research approach involves the development and analysis of unique multilayered (ML) thin films using Al and Ag. These films combine the optimum properties of the individual materials to create bilayers which compensates for the optically limiting factors of each individual material. Therefore, unlike attempts to produce AlAg-based alloys, the focus herein is on multilayered structures of laminated bilayers. This allows each material to maintain its distinctive properties, resulting in the superposition of both properties in a single thin film. For example, we wanted to figure out if it was possible to concatenate the optical and electrical properties of both Al and Ag while obtaining exceptional microstructure (surface, grain size, and grain boundaries) into a single thin film. At this stage, enough data was gathered to design an Al/Ag ML composition with enhanced reflection/transmission and microstructural properties.

Methods

An AJA international sputtering system was used to sputter-deposit thin films on circular thin-glass substrates and square-patterned grids. The deposition system used features confocal sputtering sources oriented at specific angles. The specially-designed deposition gun chimney and shutter along with a physical rotation of the sample holder stage results a relatively high degree of deposition uniformity on 4” substrates, which are over twice the target diameter (2”). Samples are

inserted into the chamber through a load-lock hi-vac chamber. The system supports up to five targets and 4 power sources, 2 DC and 2 RF (Figure 48), and one of the RF sources is used for sample biasing, which can be used for surface cleaning of the samples prior to deposition. The system is fully automated, enabling synchronous multiplayer thin film deposition with consistent results for different depositions.

The Al/Ag multilayers compositions were sputter-deposited on 18 mm glass substrates with no patterns. The base and processing pressures were ~ 1.6 x 10^{-7} Torr and ~ 5 mTorr, respectively. The sample holder was rotated at ~ 20 RPM to minimize thickness gradients across the thin film. The substrate was prepared using Ar^{+} ion milling RF power for 5 minutes to smooth the surface and clean any residual debris prior to material deposition. This part is essential so that the surface roughness and uniformity of the material is not impacted by surface contaminations on the substrate. Both Al and Ag were DC sputtered at room temperature with sputtering rates of 0.442 Å/s and 0.445 Å/s, respectively. The rates were determined via AFM scanning on photolithography-based thin-film features. A 5 min pre-deposition process was used for both materials to stabilize the sputtering rate and ensure uniformity. The layers were deposited by opening and closing the shutter using timing mechanisms to precisely measure out the desired layers of 22.6 nm for Al and 19.4 for Al. This process was repeated until the desired layer compositions were established.

Results and Discussion

The surface features of the sample compositions were analyzed to understand the grain sizes, grain boundaries, grain height range (Z) and average surface roughness (Ra). As predicted, our deposited aluminum thin films exhibited relatively large grain sizes and grain boundaries, non-uniform grain

structures, and a relatively large surface roughness. The single layer Al had a measured Z of 44.5 nm and Ra of 4.93 nm, which shows that this material is indeed rough and granular. On the other hand, the single-layer silver measurements were approximately half of Al with a Z of 20.2 nm and an Ra of 2.3 nm. When comparing the single-layer Al and Ag surface properties using AFM, it is observed that the latter is significantly smoother and more uniform which confirms the initial hypothesis regarding the single layer surface properties of each material. The combined layering of three stacks of Al/Ag showed an improved roughness with a Z of 35.5 nm and an Ra of 3.39 nm. The demonstrated reduced surface roughness compared to single-layer Al and the multilayered Al/Ag highlights the success of the surface topography improvement through interface layer design.

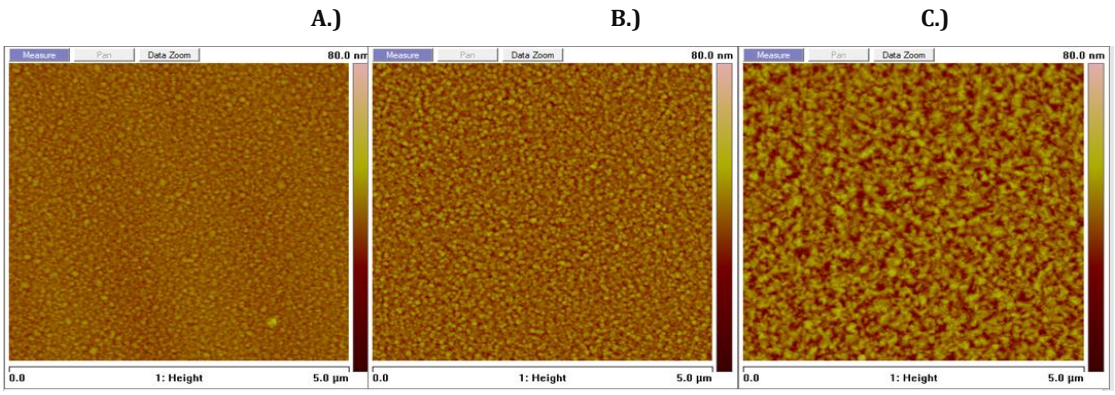

Figure 17 Each image is of the AFM surface roughness analysis of the thin film. A.) Ag 126 nm B.) Al/Ag 126 nm C.) Al 126 nm.

The next step was to analyze the sample with SEM imaging to determine the granular structure of the material based on grain boundaries and thus further understand the structure of the composition, Figure 19. The grain boundaries of the Al are well-defined and are relatively wide. In contrast, Ag had relatively tight grain boundaries that with relatively uniform grain sizes. Further review of the combined composition of the multilayer samples confirmed that the composition shows that the grains of the Al/Ag are at higher surface density and more uniform when comparing to the single-layer aluminum.

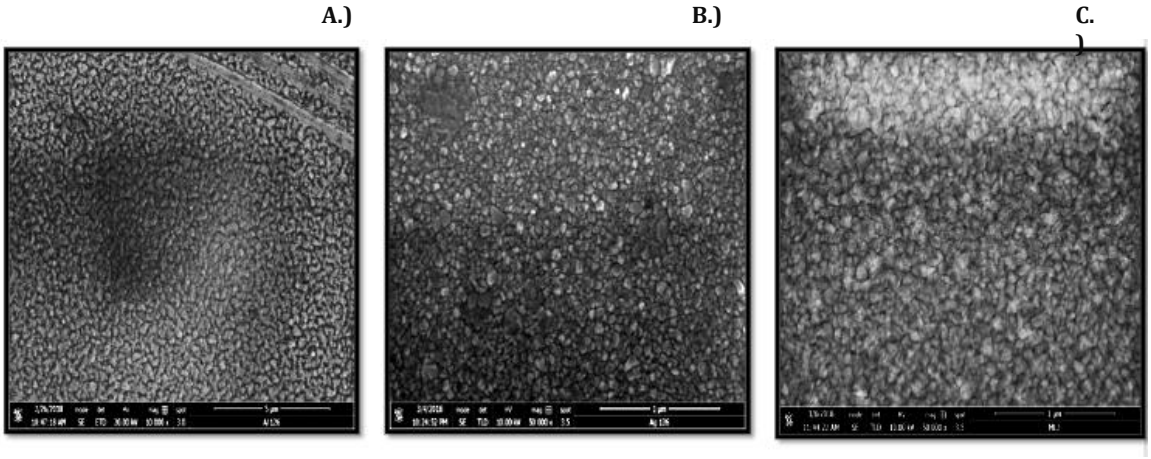

Figure 18 A.) Al 126 nm, B.) Al/Ag 126 nm C.)Ag 126 nm. Each image is of the SEM grain boundary analysis of the thin film.

A stack of 3 Al/Ag with and without an Al capping layer were further analyzed to understand the grain structure of the materials. The SEM images in Figure 19 and 20 shows the top-most capping layer looks like with SEM imaging. The figures are on the right are taken at higher magnification to reveal more clearly the difference between the thin films. The Ag top layer has smaller grains that are different from that of a single Al layer of 126 nm thickness. This shows that the Al/Ag ML thin film composition displayed enhanced microstructural properties because of a potential mismatched grains and grain boundaries between the layers of the Al/Ag ML composition. This shows that multilayering is an effective method to change the surface properties of materials.

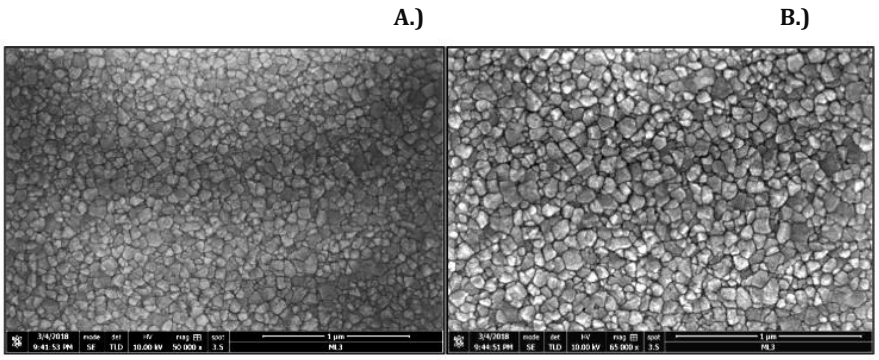

Figure 19 SEM image showing the grain boundaries of the Al/Ag multilayers with Ag as the capping layer.

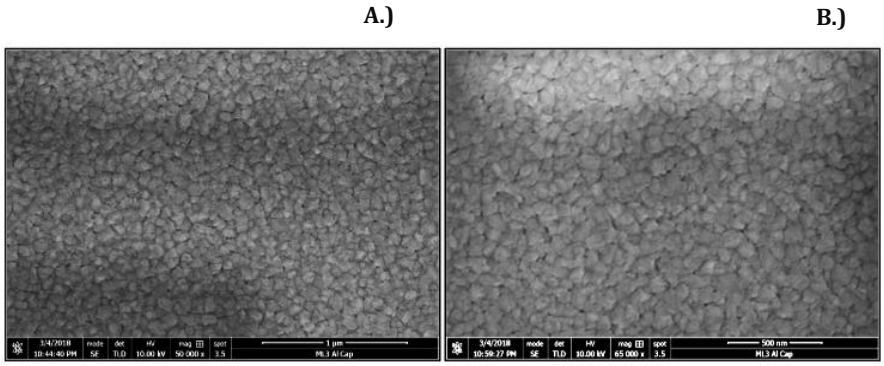

Figure 20 SEM showing the grain boundaries of the Al/Ag multilayers with Al as the capping layer.

An optical spectral analysis was performed using a Jasco J-815 CD spectrophotometer with a scan range of 180 nm – 800 nm to analyze the transmittance, absorbance, and reflectance properties of the samples. It is important to understand the optical properties of a thin film in terms of transmittance and reflectance since these relate to the phenomena of light escaping and scattering during NSOM imaging process. The samples used have different compositions of Al/Ag with ~126 nm thick films on both the thin film side and the glass substrate side to understand the saturation that occurs at about 270 nm with the glass. In all samples, the glass transmittance and reflectance became saturated at a wavelength of ~270 nm.

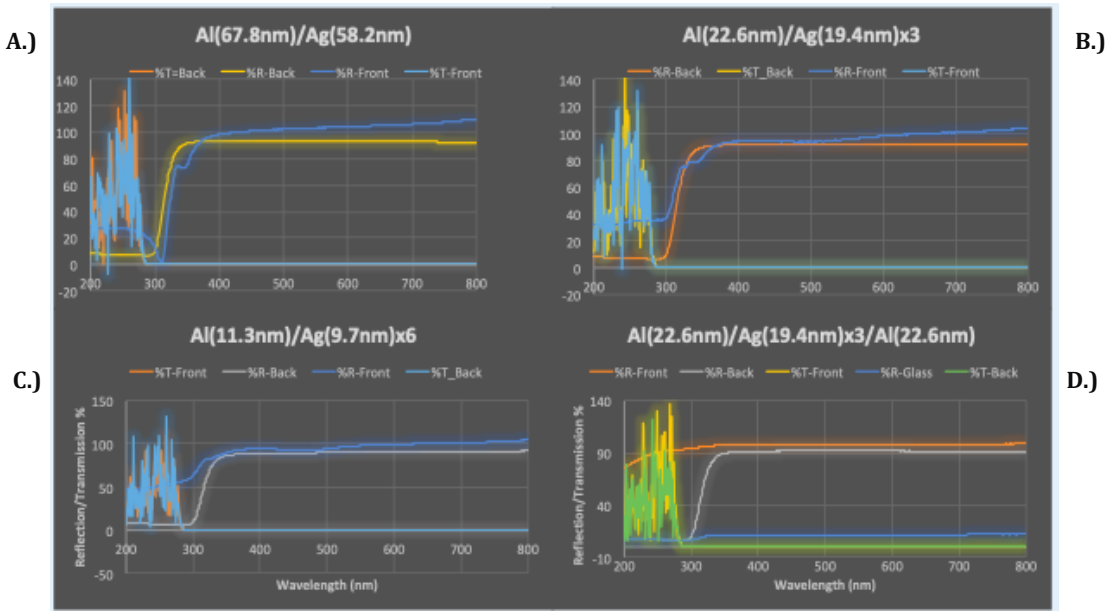

Figure 21 CD spectrophotometry results of an Al/Ag composition with an Al thickness of 67.8 nm and Ag of 58.2 nm.

The goal is to create a material that has minimal loss across a broadband spectrum of light. As shown previously, both aluminum and silver have losses at different points in the spectrum. The first sample was Al (67.8 nm)/Ag (58.2 nm), which displayed over 100% reflectance, which shows that the reflectance of the sample is superior to the mirror used to calibrate the system.

The next sample analyzed was {Al (22.6 nm)/Ag (19.4 nm)}x3 which showed that the reflectance from 800 nm – 500 nm was greater than 100%, and there was an initial drop at ~350 nm. A significant drop at ~325 nm occurred where it reached 0% reflectance, and then returned to 25% at ~280 nm. This sample showed excellent promise for measurements in the infrared spectrum.

The third composition had layers that were half the thickness of the previous sample and increased the total layers to 6, to obtain a composition of Al(11.3 nm)/Ag(9.7 nm) x6. This resulted in the transmittance remaining 0 percent, but the reflectance changed. The reflectance remained above

100% until ~580 nm and then began to steadily decline until a significant drop occurred at ~320 nm with a 70% reflectance, before levelling off at 50%. Of the 3 compositions that use Ag as the top layer, this material performed the worst at wavelengths near 350 nm by only a small margin. However, this material significantly outperformed the other Ag-capped compositions in the sub-300-nm regime by maintaining a reflectance of 50%, while the other compositions dropped well below this. For instance, Al/Ag x 3 dropped to 0% reflectance in this same region.

The final composition analyzed was Al (22.6 nm)/Ag (19.4 nm) with a 22.6-nm thick Al capping layer which also maintained low transmission. The reflectance remained over 100% until the ~ 300 nm range where it began to slightly decline until reaching a final measurement of ~80%. This sample significantly outperformed all the other compositions, as expected. When compared to Al and Ag reflectance, it was able to improve the losses observed at different points in the spectrum. This sample performed as it was designed since it showed significant optical improvements. It is critical to note that the reflectance measurement from the glass side showed properties like the one obtained from aluminum. From a layering observation, this may be of surprising differences since both the bottom and top layers have the same composition of an Al layer before a Ag layer. Nevertheless, the firstly deposited Al layer exhibits granular structures like pure Al thin films with relatively large grain sizes and boundaries, while the top-most Al layer is deposited on a silver layer that induced an improved granular structure of the that aluminum layer and thus the enhanced optical reflectance properties, Figure 22.

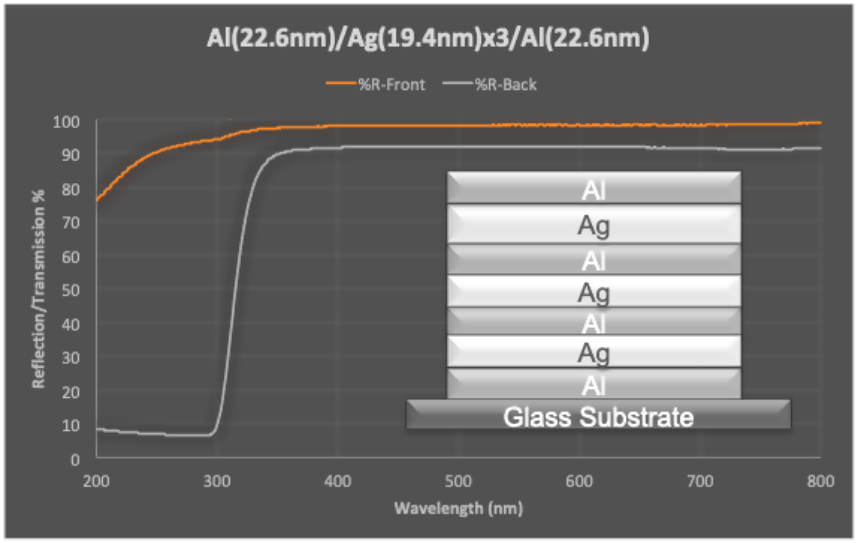

Figure 22 Spectrophotometer results of (orange line) Al/Ag with 3 bilayers and (grey line) a capping layer of Al and its spectrophotometry results.

Discussion

The obtained data shows that the proposed nanomaterial produces relatively smaller grain sizes, higher grain density, lower roughness, better uniformity, and higher predictability while still exhibiting outstanding optical properties. The surface roughness improvement for Al/Ag MLs was revealed as the top layer had a significantly lower surface roughness than single layer Al. However, when compared to the Ag capped MLs it was significantly rougher. This leads into the reflectance data showing significant improvement with the Ag capped MLs and the Al capped composition. The improvement was significant until entering the sub ~ 300 nm wavelength of light range, where the Ag capping layers dropped significantly when compared to the Al capped layer; however, they still outperformed the single layer Ag. At lower wavelength of light electrons oscillation will be reduced causing the radiative field generated during specular reflection to be weaker, which then allows more light to penetrate the sample. The grain mismatching did cause more scattering but with the Ag capped layer, the many interfaces allowed for light to penetrate the different layers.

Conclusion

The goals set out to accomplish of an optically improved material for NSOM was achieved. By first decreasing the surface roughness of the aluminum the optical performance significantly improved. The Ag capped ML did show significant promise in the UV range and above, as the reflectance exceed 100 percent, which is better than the mirror used to calibrate the machine. Next, it was proven to hermetically seal the Al layer which leads to future work to use this material as an electrical contact. Most significantly, the data presented shows the potential for further optimization of MLs based on Al thin films to produced enhanced aluminum thin films with improved microstructural and as a result also improved optical proprieties.

Magneto-Optical Characterization of YIG Thin Films via Faraday Effect in both Out-of-Plane and In-Plane Directions

Introduction

Yttrium iron garnet (YIG) is a ferromagnetic material that has garnered a substantial amount of attention in the spintronics community for its low damping and electrically-insulating behavior [52]–[55]. Its minimal damping gives the material a more stable magnetic field signal and a higher energy efficiency, without external interference [56]–[58]. Its electrical insulation properties give the material magnetoresistance by restricting the flow of electrons, which increases its thermal stability [59]–[61]. The overall benefit of these properties is to increase the efficiency of the material in low-power electronics and radio frequency (RF) applications. Using the Faraday effect, the hysteresis of YIG can be determined, while characterizing its magnetic properties allows the anisotropy and the coercivity of the material to be used to confirm its fundamental properties as an energy-efficient and magnetically-stable material [62], [63]. Since the required external field for the resonance is much higher than the anisotropy fields of YIG, the accuracy with which the anisotropy constants can be determined is limited.

The typical technique to map the magnetic domains of YIG is ferromagnetic resonance (FMR) spectroscopy, which has shown excellent results when used to investigate the internal magnetic field in magnetic materials and has become the standard method for characterizing magnetic-based anisotropy in thin films. The typical setup includes a band cavity resonator, which scans the surface of a thin film and produces constants by fitting the data to a predetermined form. However, this

method requires a long data processing time, and it can be physically aggressive and degrade the quality of the sample.

In this work, we focus on characterizing magnetic field using the Faraday effect measurement by analyzing the angle of light when it enters the material. This method of characterization allows for the material magnetic domains to be mapped without any physical contact or alterations and can also map the YIG domains in fashion like FMR, however it uses a different methodology. The MOKE system was configured in transmission mode and thus produced a signal directly proportional to the magnetic moment along the out-of-plane direction of the thin film and throughout the whole substrate. Since the GGG substrate exhibits paramagnetic behavior, a background linear Faraday-rotation signal was superimposed on the magnetization signal of the YIG and YIG+YIG structures. This signal was subtracted in some plots to place more emphasis on the magnetic properties. Various measurements were conducted through selected regions of the pattern cross feature sample to investigate the uniformity of its magnetic properties. The sample was further investigated with AFM/MFM to validate the data. Finally, magnetic properties of the features were confirmed by investigating the uniform sample along the in-plane direction using longitudinal Faraday-rotation analysis.

Experimental Setup

The fabrication process of the YIG cross junction involved making a single-crystal YIG film grown on top of a gadolinium gallium garnet (Gd3Ga5O12) substrate using the liquid-phase epitaxy technique. Micro-patterning was performed by laser ablation using a pulsed infrared laser ($\lambda \approx 1.03$ μm), with a pulse duration of ~256 ns. The experiment used the MOKE system to measure the Faraday effect and to confirm the magnetic direction of the material, which has excellent Faraday

rotation and allows light to be transmitted. The transmission mode of the MOKE was used, where the laser shines through the sample into a detector that measures the signal in one of two transmission modes: longitudinal or perpendicular. The longitudinal mode is shown in Figure 24, where the laser is shined into the sample at an angle along the sample in the direction left or right where the field is pointing. In the perpendicular mode, the sample is perpendicular to the laser and the magnetic field, and the perpendicular media points up and down. The quality of the material is determined using this measurement.

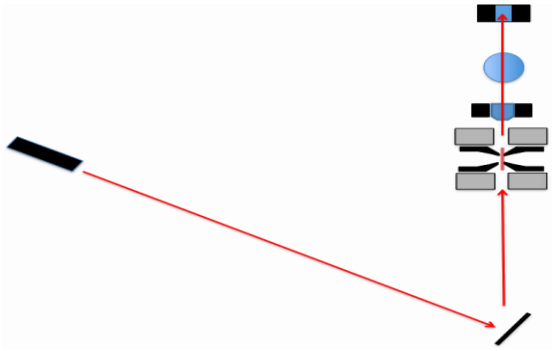

Figure 23 Longitudinal MOKE set up.

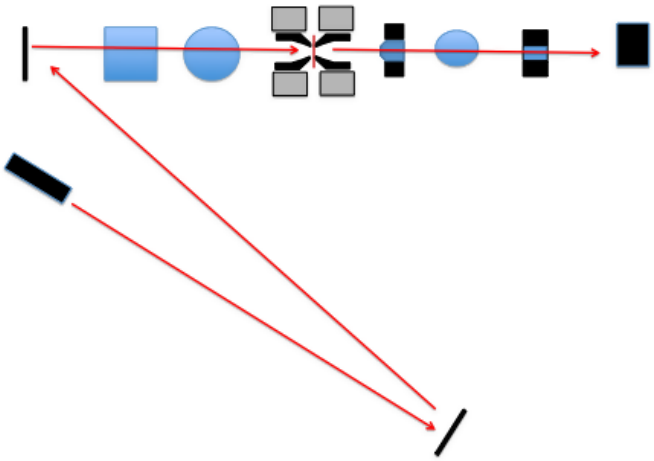

Figure 24 Perpendicular MOKE set up.

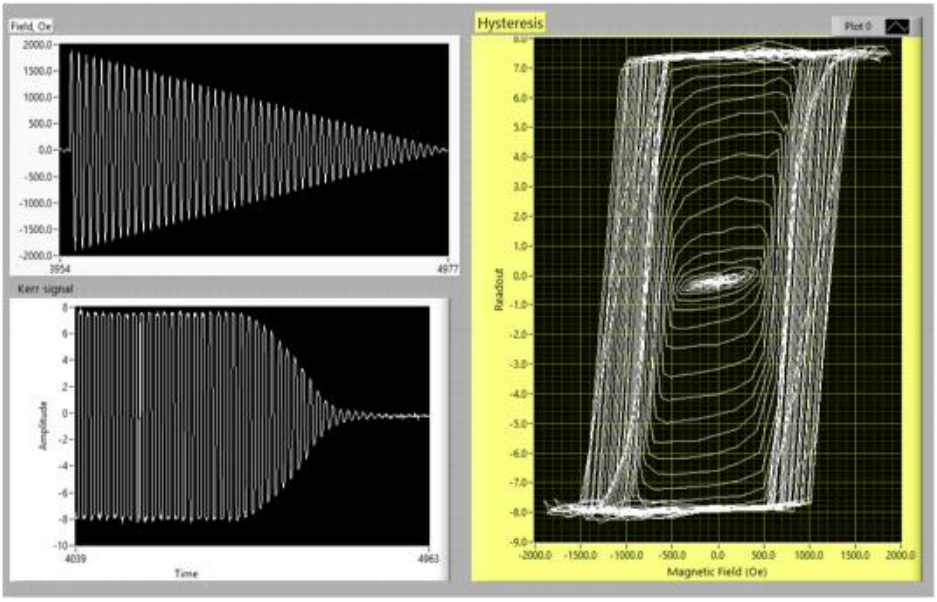

Figure 25 Calibration of the MOKE system using cobalt and palladium multilayers.

Results and Discussion

One of the corresponding figures indicates the Faraday Rotation (also referred to as the transmission magneto-optical Kerr-effect [MOKE] microscopy) configuration for which the sample was analyzed. A laser source producing red light with a wavelength of approximately 630 nm was used to investigate the YIG-based structure. The laser spot was focused to a diameter of about 30 μm to analyze the feature sample and collected via an objective lens embedded within one the electromagnet's poles.

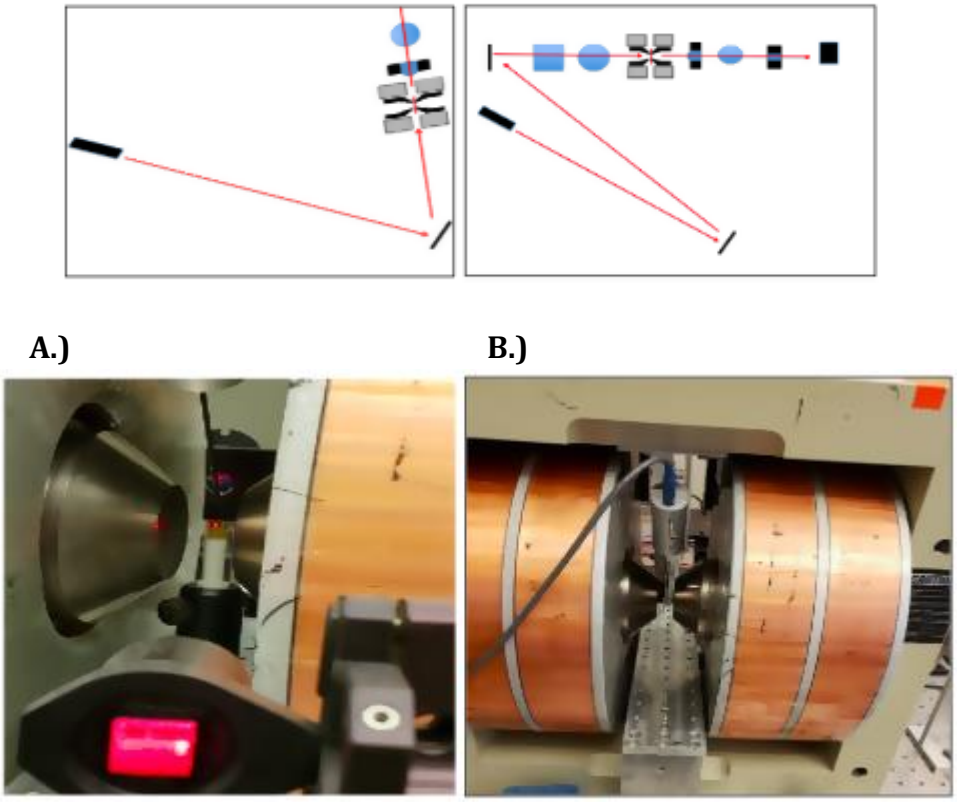

Figure 26 A.) Shows that YIG sample set in Longitudinal mode B.) This is the YIG sample set up in Transmission mode

The MOKE system was configured in transmission mode so that it produced a signal that was directly proportional to the magnetic moment along the out-of-plane direction of the thin film and throughout the whole substrate. Since the GGG substrate exhibits paramagnetic behavior, a background linear Faraday-rotation signal was superimposed on the magnetization signal of the YIG and YIG+YIG structures.

A.)

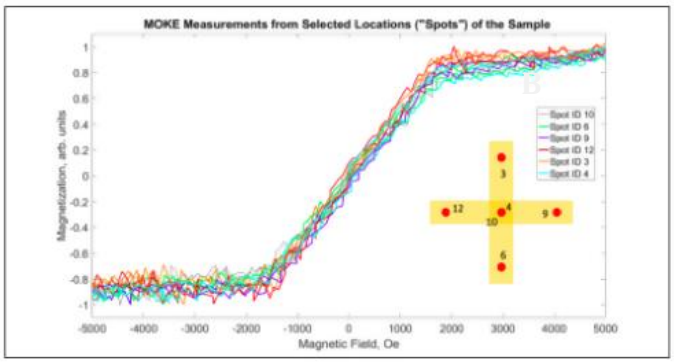

B.)

C.)

Figure 27 A.) shows the hysteresis of curves at different points located in the diagram on the patterned substrate. B.) The sample loaded in the holder clearly showing the cross pattern. C.) The sample loaded in Transmission mode for measurements.

The sample in figure is an unpatterned sample of a YIG film on a GGG substrate. The composition layers vary at different points on the sample, including GGG/YIG/YIG, GGG/YIG, and GGG. These multilayers are expected to have different hysteresis effects. The experiment on the unpatterned sample was performed by pointing setting the parameters at a constant for the external magnetic field. As seen in Figure 29, the measurement locations are labeled 1-6 with a 0.25 mm space between each measurement. The sample showed no difference in the hysteresis throughout the several locations, indicating that this sample had a high probability of being longitudinal.

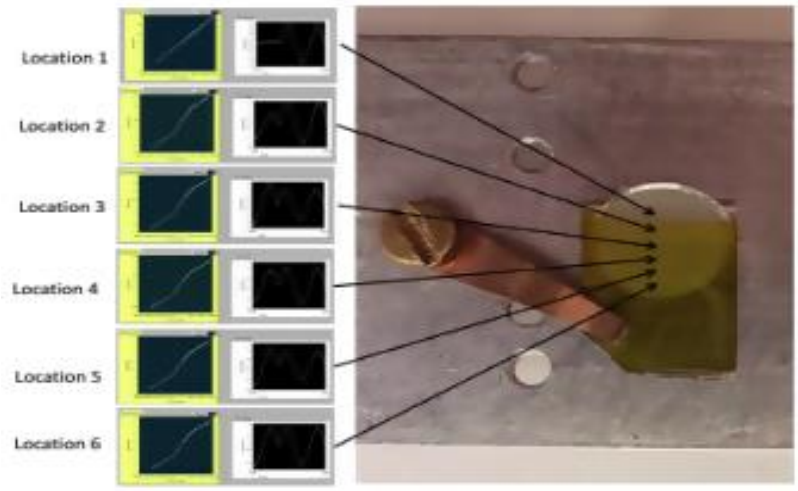

Figure 28 The hysteresis point were taken at different locations on the unpattern YIG sample at different layer compositions.

The MOKE shown in figure was configured in the longitudinal mode, as it was determined that this was the direction of the magnetic domains. The unpatterned YIG sample was used for these measurements, since it covered the entire substrate, which made it more practical to measure using this system. The measurements were taken at 3 different points which corresponded to the three different composition layers of YIG. The hysteresis of this sample at the different layers showed a difference, which confirmed that the material was a longitudinal media.

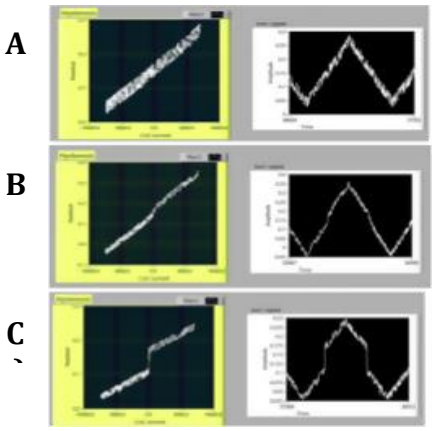

Figure 29 The hysteresis plots of the unpattern YIG taken in longitudinal mode A.) GGG B.) GGG/YIG C.) YIG/GGG/GGG

MFM measurements were performed on the sample to determine if the magnetic domains could be mapped out. The patterned substrate was measured by MFM at 5 different locations, located at the 4 ends of the cross points and at the center point of the pattern. The patterns in the sample could only be resolved using AFM, as these patterns showed minimal to no reaction in the MFM system. As shown in Figure 31, the material generated a surface analysis with the AFM that shows the grain structure and surface roughness, compared with a standard magnetic sample of Co/Pd. The MFM also showed that this is a demagnetized sample since the randomized magnetic domains were pointing both up and down.

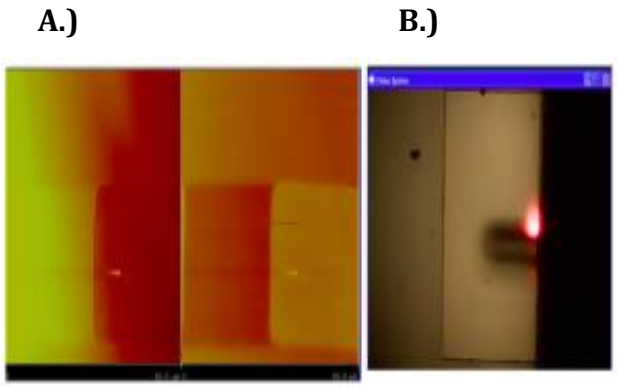

Figure 30 The figures compares the MFM field of the patterned YIG sample. A.) The unflattened AFM and MFM images a selected pattern of the YIG sample B.) A photo of the location of scan

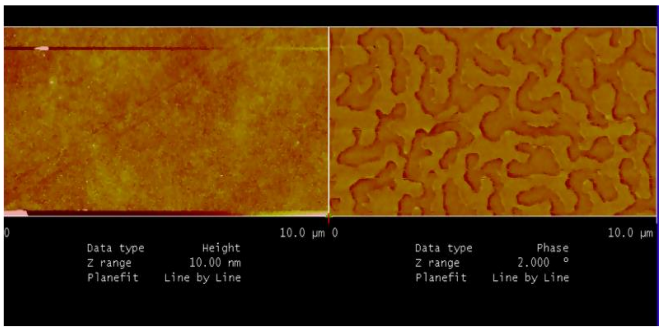

Figure 31 Standard MFM image of cobalt and palladium multilayers with demagnetization of the domains.

Conclusion

The obtained magnetic hysteresis measurements indicated that the YIG thin film had a preferred magnetization in the longitudinal direction (along the plane of the feature). Furthermore, the results indicated uniform magnetic behavior throughout the key points of the structure with an anisotropy field H_k of about 1.9 kOe. Therefore, during spin wave measurements, it is enough to apply a magnetic field of about 2 kOe to align the sample magnetization in any preferred direction. Any

excessive field will only introduce background noise from the GGG substrate. The AFM data showed patterns with dimensions of about 20 um x 20 um with a pitch of 20 um. These patterns may well be the cause for the variation in the Faraday-rotation signal at the different feature locations. The MFM data didn't reveal any noticeable magnetic domain for these features, so signal domain behavior may be assumed. It can be assessed that this is a low anisotropy and high coercivity material, making it highly energy efficient and an excellent choice for low-power electronic applications.

The Future of Data Storage

The growing need for larger capacity, higher density, and more cost-effective digital data storage devices

Magnetic memory storage based on HDD technology has been the focal point of the data storage industry since it was founded, and more recently with the development of solid-state drives (SSD) with terabyte memory capacities. The need for HDDs has not decreased due to their high storage capacities and lower prices which SSDs cannot compete with. The market for high-density memory storage is expected to quickly exceed peak 2014 demands by 2020. The capacity has also been predicted to exponentially increase as the demand for more storage per bit meets the predicted road map. The growing market for HDDs began with the emergence of personal computers (PCs) and has continued to rise for the past four decades. However, a new market is emerging that requires large data centers to support the internet of things (IoT), cloud-based storage systems, mobile devices, cryptocurrencies, and HD and VR gaming. HDDs are still needed to support the memory requirements for these emerging technologies.

New devices, especially SSDs are integrated into technology to better support the growing need for not only higher density but faster memory. The constant need to find new solutions for the continual scaling of this technology has many caused drastic shifts in the last decade. During the initial decades, the use of longitudinal-based media dominated, but this has shifted to perpendicular media the last 10 years. The need for faster access to memory has shifted the market from perpendicular magnetic media to SSD. However, SSDs have their shortcomings such as limited storage capacity for the price, as well as their limited lifetime cycles, so a hybrid methodology has been used to

incorporate the technology into most PCs. Due to the fundamental limitations of longitudinal and perpendicular magnetic recording, together with the ever-increasing demand for higher information storage capacity, both the industry and research groups around the globe have been forced to develop alternative technologies to further advance the current state of conventional technologies.

How Does Magnetic Recording Work? LMR vs. PMR

After many years of research, the memory storage industry has optimized HDD technology by focusing on longitudinal magnetic recording (LMR), which has excellent reliability, efficiency, speed, and areal densities, which allowed it to meet industry demands for decades. This technology remained the primary method for the industry until the fundamental superparamagnetic limit was reached [64], [65]. This technology was the staple of the industry until a decade ago, when the technology shifted to perpendicular magnetic recording (PMR).

Traditional LMR operates by scanning the surface of the HDD with a read/write head inducing a magnetic state, which creates a bit. The material is a single-layer magnetic thin film that has many different grain boundaries and magnetically-randomized domains until the write head changes the state. The reason it is defined as longitudinal can be seen in the figure 33 the magnetic domains point left or right along the material surface. This structure consists of bits which are a grouping of magnetic grains that point in the direction specified by the read/write head. In longitudinal recording, the media encompasses grains which are randomly-magnetized within the plane of the media. Each bit encompasses about 40 - 100 grains to statistically ensure bit stability and readability [66]. This fundamental limit is caused by thermal instabilities in the recording media when the physical bit dimensions are reduced below certain fundamental values. In short, this limit indicates

that in longitudinal recording systems, recorded bits of information are not stable at room temperature if the areal density surpasses about 200 Gbits/in^2 [67]. This has resulted in the HDD industry moving towards become the current standard method of PMR.

Perpendicular recording works by shifting the magnetic domains up and down, as shown figure 33. This allows for a higher grain density, scaling down of the bit size and thus, the modern replacement for traditional LMR technologies is the PMR method [68]–[70]. The two primary changes of this technology are the read/write transducer and the composition of the thin film material used for magnetic media. There are two factors that permit the use of higher-anisotropy materials with greater volume per grain, which leads to a greater areal density. First, a soft underlayer (SUL) is added, which consists of a soft magnetic material deposited below a hard magnetic material which doubles as the magnetic recording layer [71]. The result is that perpendicular recording of the magnetic field flows in a closed magnetic circuit in the presence of the SUL.

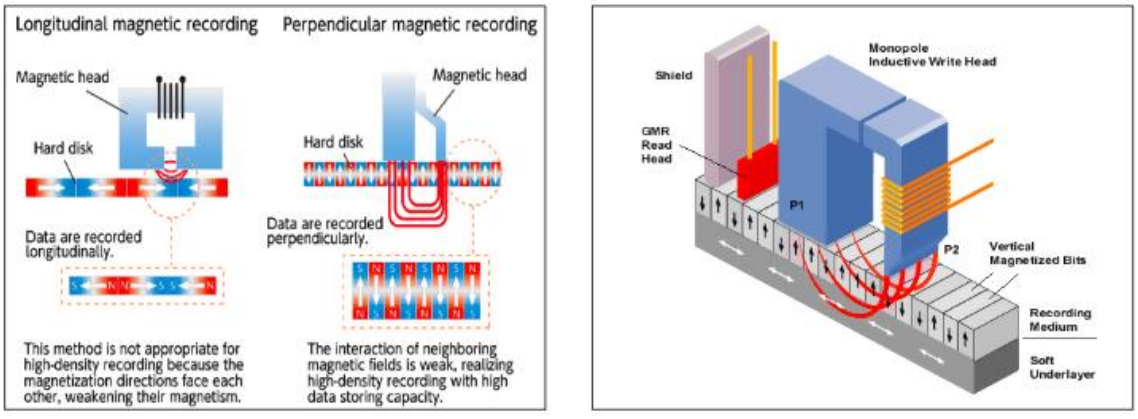

Figure 32 Schematic of the LMR and PMR and how the bit pattern media is read on a hard disk drive

The Superparamagnetic Limit

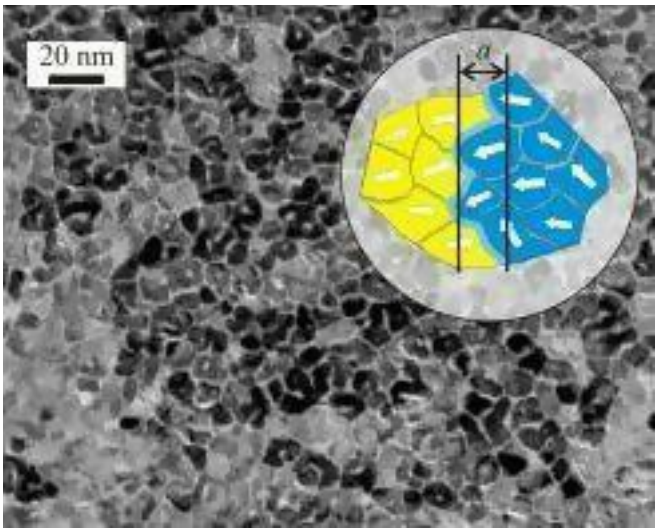

Figure 33 This SEM Image is showing the scattering of the magnetic domains due to the super paramagnetic limit being reached.

The superparamagnetic limit is a form of magnetism which appears in small ferromagnetic or ferrimagnetic nanoparticles. The magnetism of the particles or grains points in a specified direction left or right in longitudinal media and up and down in perpendicular media. As the bit size decreases because of continual scaling demands on performance, the magnetic moment around the bit becomes more unstable. In sufficiently small nanoparticles, magnetization can randomly flip direction due to temperature. This issue arises based on the Signal-to-noise log(N), where in *N* is the number of grains per bit. This leads to a constant number of grains being maintained as bit dimensions are scaled down.

Since the number of grains must remain constant, the only way to achieve higher areal densities is to reduce grain volumes. This can lead to adverse effects caused by thermal fluctuations in magnetic media, such as the flipping of magnetic directions, instability, and corrupted data [6]. The way for

this field to evolve is for it to remain vigilant and develop measures that account for the super paramagnetic limit.

Current Developments in Magnetic-based Data Storage

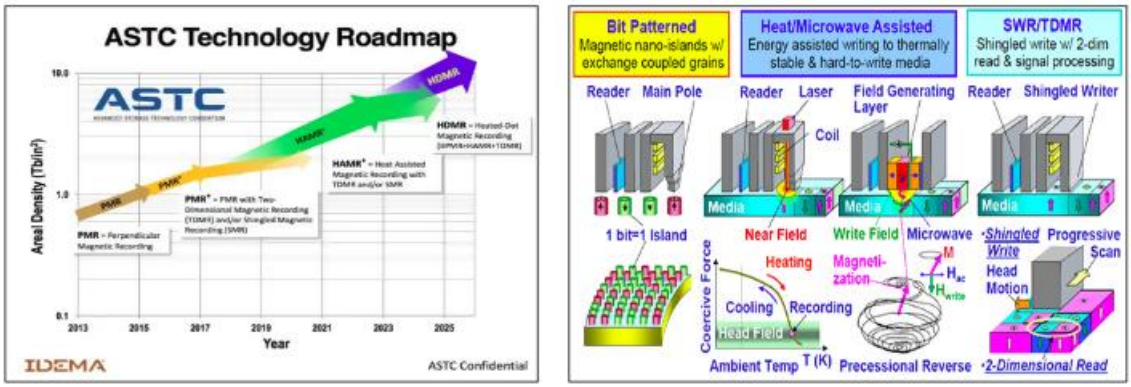

Figure 34 The left image details the continual scaling of HDD storage over time. The image on the right details near-future technology to enable the continued use of conventional HDDs.

Future Technologies in HDD

HAMR

Heat-assisted magnetic recording (HAMR) can facilitate the use of higher anisotropy materials, which can lead to a higher thermal stability [72],[73]. As its name implies, to record information, HAMR relies on using not only magnetic but also thermal energy by applying a laser beam that heats designated areas where media is being recorded, and a final field is applied after this process. In other words, both thermal and magnetic energies are combined to switch the magnetization. Therefore, a hybrid write/read system that uses both heating and magnetic sources is used to record

on high-anisotropy magnetic media [74]. The write field required to switch bit magnetization and the stability of the bits are both directly proportional to the media's anisotropy energy density, which limits the recording media to compositions with lower anisotropy [75]. On the other hand, magnetic coercively, which is the ability of a ferromagnetic materials resistance to demagnetization by and external magnetic field, dramatically decreases as the temperature increases. Local temperature increases in the regions where magnetics domain exist requiring sufficiently small fields to switch the magnetization despite the ultra-large anisotropy of the recording media [76]. Nonetheless, there are numerous obstacles that must be overcome before such a technology can be realized, specifically the integration of a near-field optical source with sufficient energy throughput [77],[78].

MAMR

Microwave-assisted magnetic recording (MAMR) uses microwaves to record information into bits. Microwaves are created using a spin torque oscillator (STO) near the write gap of the recording head to lower the magnetic field of the media. An advantage of this method the ability to use conventional PMR with an SUL, which enables it to be integrated with current technology. One interesting use of MAMR is selective material interactions, since it was shown that MAMR only interacts with specific hard materials and has only a minimum effect on the soft magnetic layer. It has been shown that MAMR affects the overwrite and the SNR improvement even with high coercivity media. However, an adverse effect is that the STO has been found to degrade the MAMR writing process by increasing jitter, decreasing LFSNR, decreasing MWW, and decreasing ADC [79]. However, these issues are much fewer than those that exist in HAMR, such as decreases in the head reliability due to heating and the cost of additional components [80].

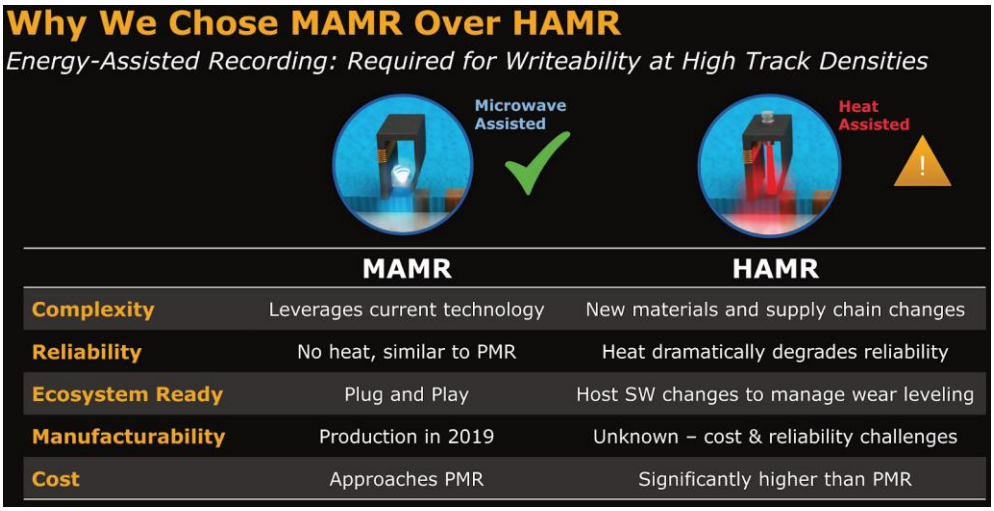

Figure 35 The advantages of MAMR over HAMR, showing why this is the future of the HDD drive.

Multilevel 3D Magnetic Recording

Two different 3D recording modes with respect to addressing separate magnetic layers will be referred to as ML 3D and absolute 3D modes, respectively. In the ML 3D mode, a 3D space is utilized for recording, but it is not used efficiently. In an example case, the signal that is recorded and read back from a vertical stack is defined by the recording head above the stack. In this case, the information in all N layers within the stack simultaneously contributes to a certain signal above the surface of the 3D media, as in Figure 40. The number of signal levels (L) is different from the number of magnetic layers (N). This number is determined by the ability of the fabricated 3D media to generate a distinct signal with adequate SNR for L levels to be distinguished from each other for which the magnetization of each layer is enough. The number of signal levels is also limited by the ability of the recording element to address each magnetic layer across the 3D media. In this case, the effective density increases by a factor of log 2L with respect to the density of the equivalent binary single-layer media. In contrast, in the absolute 3D recording mode, each n-th layer in the N-

layer recording media could be addressed separately, Figure 36, via some physical process (to be explored). In this case, the effective areal density would increase by a factor of *N* with respect to the areal density of the equivalent single-layer media. For example, if one thousand layers are used, assuming a bit cell cross-section of 160 x 160 nm^2, 25 terabits of data could be stored in one square

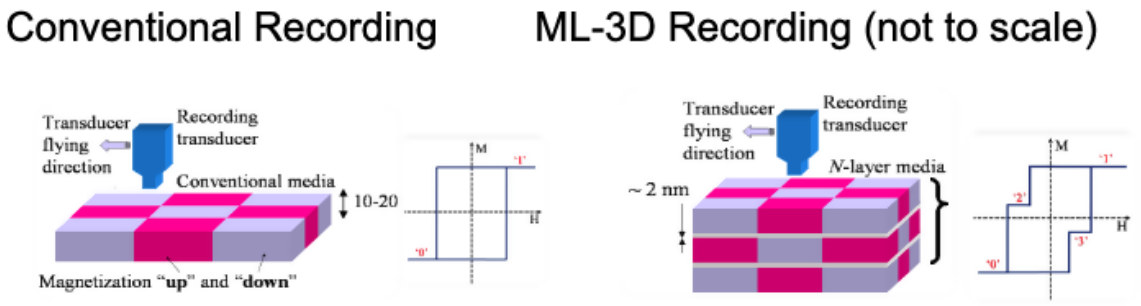

Figure 36 ML 3D media schematic and how it functions compared to traditional single-layer media.

Potential Co/Pd dual-stack magnetic media with dielectric (SiO2) separation layer for both electric and magnetic isolation.

Introduction

The goal of this research is to develop a magnetic thin film that contains two magnetic layers which are both magnetically and electrically decoupled so that an electrical current can be passed through one layer without affecting the other. It also means that the magnetization of each magnetic layer can be switched without affecting the magnetic state of the other layer. Extensive research has been performed on the development of such thin films using only a magnetic isolating layer, but little research has focused on using both electric and magnetic together. An investigation is currently underway to assess the potential of using SiO_2 for this purpose which will study other dielectric materials such as Al_2O_3, TiO_2, MgO, and a semiconductor Si. The magnetic composition of each layer is currently being optimized and encouraging results are being obtained for the SiO_2 composition.

To obtain perpendicular magnetic media requires a magnetic crystal structure to be oriented in such a direction. It usually requires significant preparation of seed layers, deposited using different deposition conditions and temperatures. The significance of using Co/Pd multilayers is their independence from the previous layer's crystal structure. The perpendicular anisotropy is caused by the interface between the Co and Pd layers and the surface smoothness of the seed layer. It is thus vital to maintain proper surface properties of the insulating layer (Dielectric 2) so that the magnetic layer (Magnet 2) will also have perpendicular anisotropy. It was thus desirable to establish

an effective and credible characterization method to analyze 3D-ML magnetic media for MAMR applications.

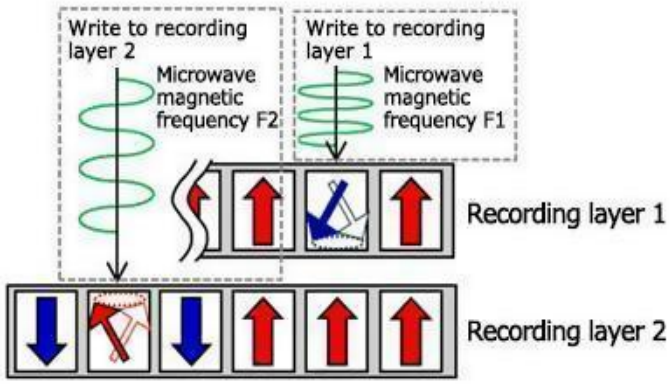

Figure 37 Illustration showing how microwaves from the read head can penetrate and interact with each magnetic recording layer.

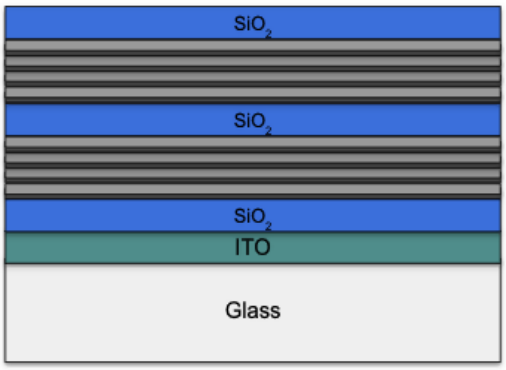

Figure 38 A diagram of the multilayer media layering

Experimental Setup

The conventional method to non-destructively characterize magnetic thin films using visible light is Polar-Magneto-Optical Kerr Effect (P-MOKE) microscopy. In this method, linearly-polarized light is directed to the thin film surface, and light that bounces back from the surface carries with

it the magnetization state of the thin film. While it is very effective for conventional single-layer magnetic recording media, this analysis measures the magnetic properties of the thin film surface with a penetration depth of about 10 nm, depending on the material composition. Since magnetic thin films are relatively thin (below 30 nm), magnetic domains do not form across the thickness of the thin films. Thus, the analysis of surface characteristics using P MOKE is sufficient to also represent the properties of the entire thin film across its thickness.

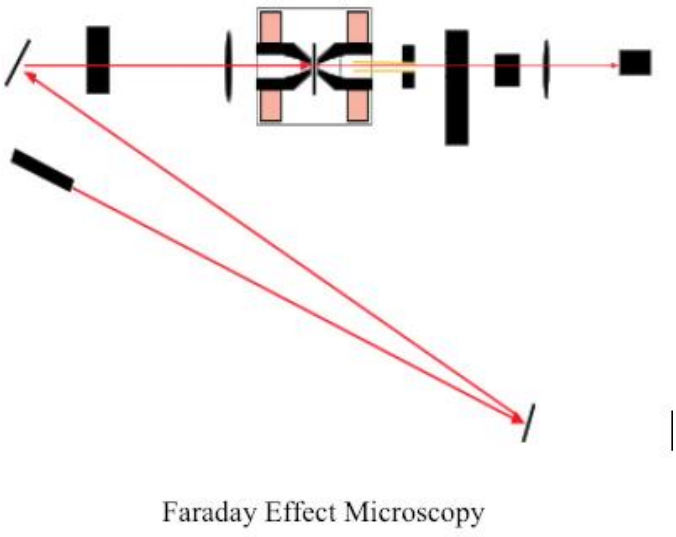

Figure 39 The MOKE system configuration for measuring FE in perpendicular transmission mode

This is not the case for 3D-ML magnetic recording media for MAMR. For this technology, at least two separated magnetic layers are needed across the thickness of the thin film. Furthermore, these layers must have stable magnetization states which are independent from each other Therefore, using only surface-based analysis by the MOKE system may not be enough to fully characterize all the independent magnetic recording layers across the thickness of the thin film. Thus, a system is needed that is based on light transmission through the entire thickness of the thin film that carries

the magnetization signals from all the independent magnetic layers. For this, a custom-made Faraday Effect (FE) microscopy system was assembled.

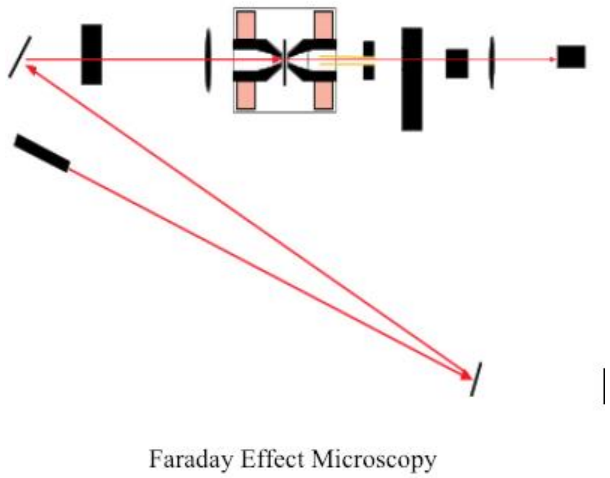

Figure 40 The MOKE system configuration for measuring FE in perpendicular reflection mode

Using the FE prevented the use of common silicon substrates and required the use of a substrate that is transparent to light, which is why glass was chosen. Thinner glass is better because it minimizes Faraday rotation of light exiting the magnetic thin film. Faraday rotation is linearly proportional to the strength of the magnetic field and thickness of the glass, and it usually gives the hysteresis loop a minor CCW rotation. The main concern with using glass substrates was its surface roughness and smoothness because of the Co/Pd thin film fabrication requirements.

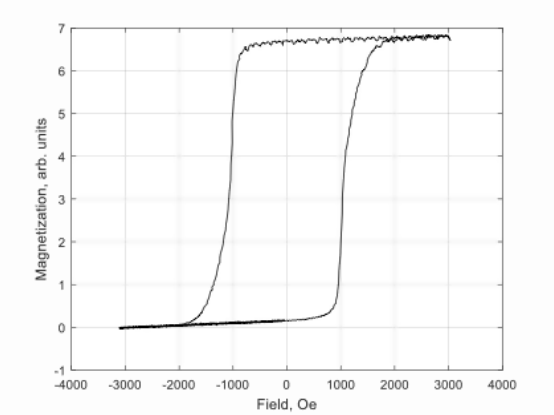

Figure 41 Example of hysteresis with a slight CCW rotation from the glass substrate.

After analyzing the glass substrate, Ar-ion milling was performed on the surface, and before each deposition the glass substrate was prepped, by cleaning it with acetone, isopropanol (IPA), and then deionized (DI) water to remove any debris or contamination. Next, half the sample was covered, and the other half was exposed. Finally, the sample was loaded into an radio frequency (RF) sputtering system, using a standard RF power of 50 watts for 5 minutes, and then the sample was removed. The sample was analyzed using AFM on both the covered and exposed locations. From the image, the smoothness of the sample was significantly improved, demonstrating that this process could be used to maintain a smooth and adhesive surface for the processing of Co/Pd films.

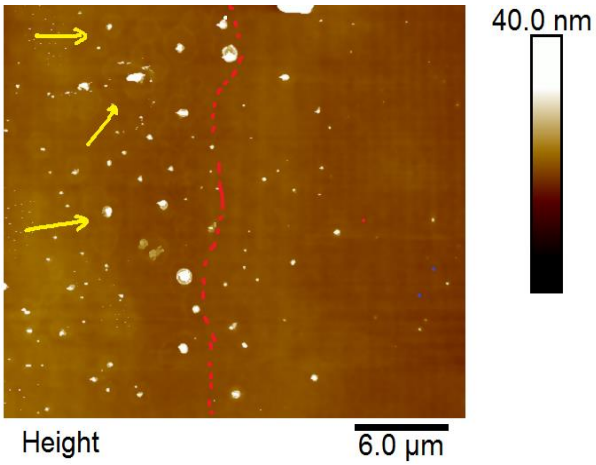

Figure 42 A glass sample displaying argon milling on one side and the original non-milled side. The surface roughness of the milled side was noticeably improved.

A single magnetic Co/Pd thin film layer was deposited to check the functionality of the system. Composition sputtering was then checked to first see if the deposition rates were accurate and to assess the quality of the material being deposited under the set parameters. The material was then deposited individually onto a patterned substrate to determine the step height. First, individual compositions were deposited to confirm the rates of Co (.327 Å/s), Pd (.408 Å/s), and SiO_2 (.417 Å/s). The rates were confirmed to be accurate, and the film was also confirmed to be uniform. A test sample of Co/Pd was then prepared to act as the standard sample to calibrate the characterization systems for the MOKE.

The MOKE test measured the coercivity of the sample by taking a continuous hysteresis of the sample, until it reaches zero. Once the zero state is reached it can be established that the system is calibrated since all measurement curves will be centered at zero. Also, for the field and Kerr signal, the up and down should be measured equally in both directions, and if this does not occur, there is an error in the system.

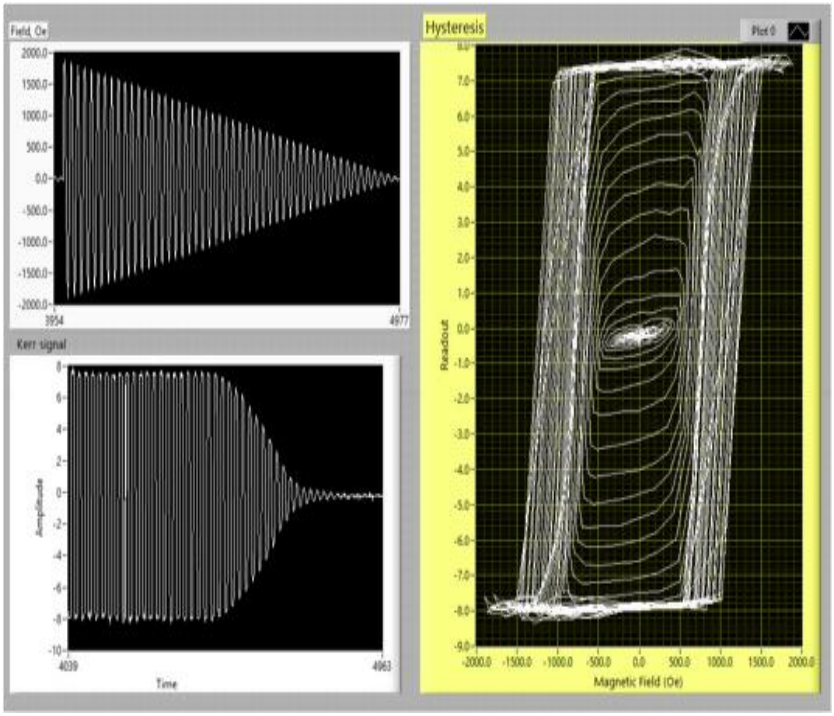

Figure 43 The Co/Pd sample used to calibrate the system to ensure there is no drift in the instrumentation that could cause offset measurements.

Results and Discussion

The investigation then continued into trying to determine the optical properties of various thin films to ensure that the 3D-ML media was suitable to be characterized by the FE system. If the 3D-ML becomes opaque, light will not transmit through it, and this analysis method cannot be used. The goal here was to use relatively transparent non-magnetic layers to ensure that the thickness of the less-transparent and vital elements of Co and Pd is maximized. Optical spectral analysis was performed on various compositions including glass substrates milled/as-is, ITO, Co/Pd, SiO_2, etc. SiO_2 was chosen since it is relatively transparent, a dielectric, and non-magnetic (and is also available for the sputtering system).

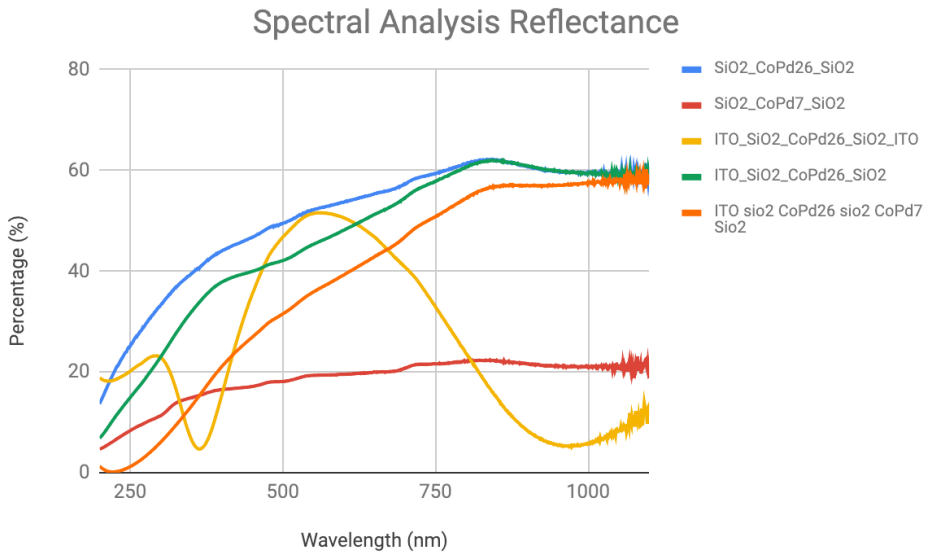

Figure 44 Spectral analysis of the reflection of the materials

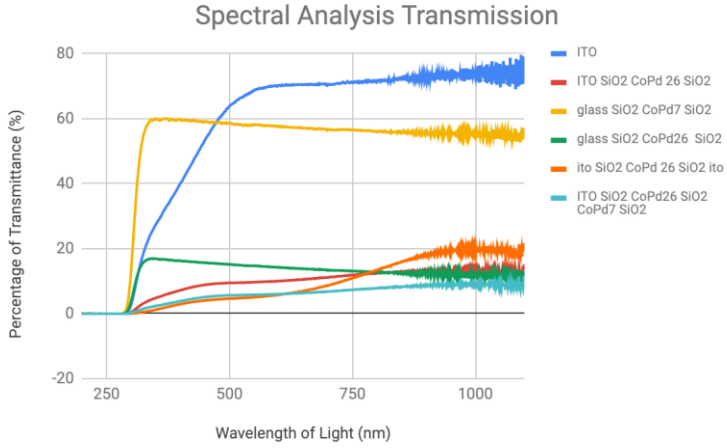

Figure 45 The spectral analysis confirmed that it was okay to use the FE system and that the light wavelength used showed the best transmission properties.

The deposition of Co/Pd single-layer media with different number of bi-layers repeats was conducted. This was done to establish distinctive properties for each layer to obtain 4 independent

magnetic states of such media: UP-UP, UP-DOWN, DOWN-UP, DOWN-DOWN. An SiO_2 capping layer was used for these thin films.

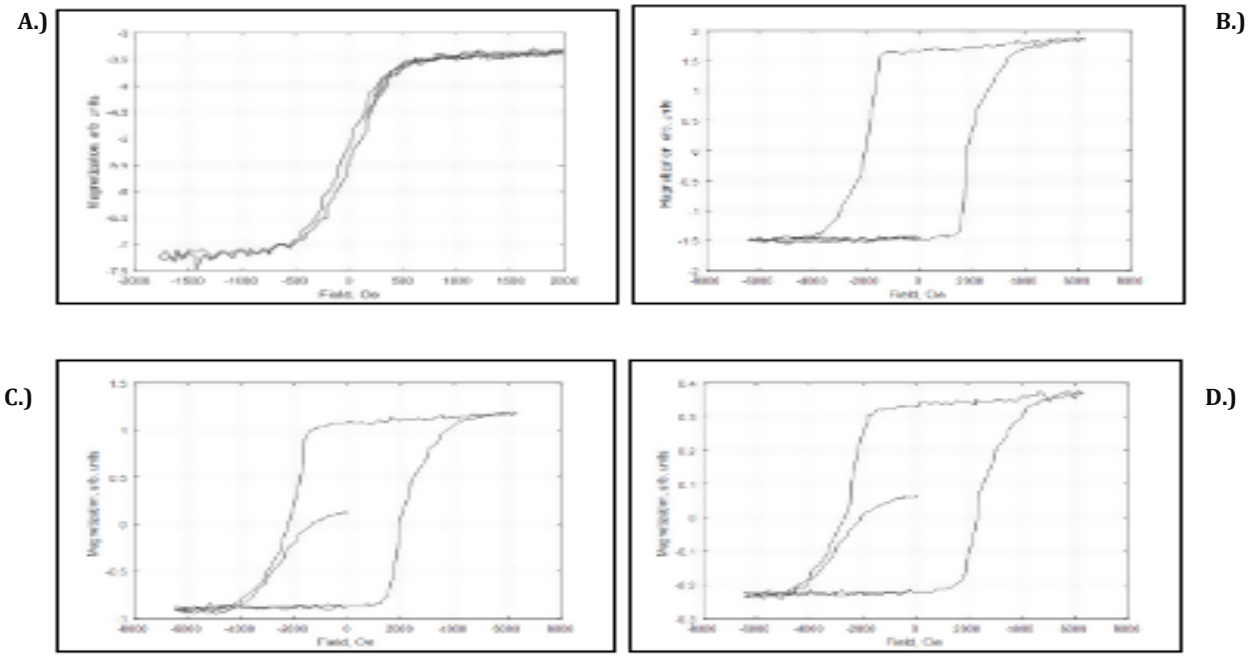

Figure 46 Hysteresis curves of different Co/Pd compositions starting from the A.) Co/Pd x 7 B.) SiO_2/CoPdx26/SiO_2; C.) ITO/SiO_2/CoPdx26/SiO_2 D.) ITO/SiO_2/CoPdx2/6/SiO_2/ITO.

The FE analysis showed that the signal from individual layers could be successfully obtained. Then, minor loops were performed to fix the magnetization of one layer (the bottom one) while changing only the magnetization of the second layer (the top one). In this case, the bottom layer required a greater magnetic switching field than the top layer so the magnetic field range was set lower than the switching field of the bottom layer, and only the magnetization of the top layer was switched.

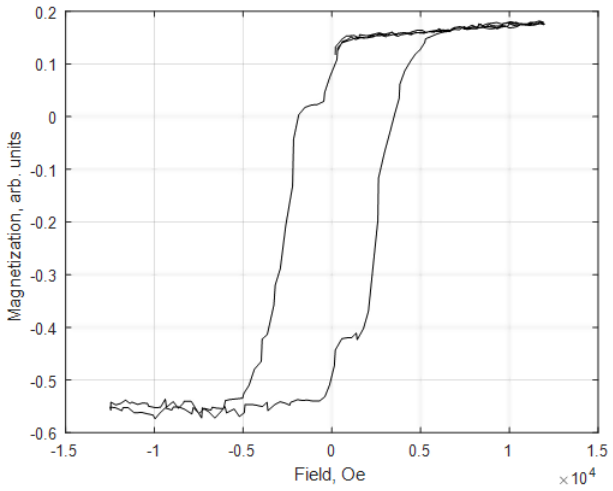

Figure 47 Hysteresis of the bi-layers

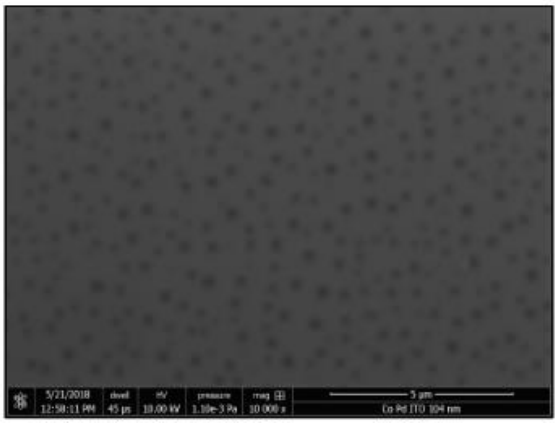

Figure 48 SEM surface analysis of the dual layer with a SiO_2 capping layer

Conclusion

The analysis revealed that the top layer is perpendicular but has a remanence magnetization of zero, which means that it cannot be used to store magnetic data. Then, an investigation into the cause of this phenomena was conducted. For this, AFM, SEM, and MFM were used, and the results showed that the SiO_2 interlayer did not bind well into the Co/Pd thin films and formed SiO_2-based

nanoparticles across the thin films. Since this eliminated the flatness of the surface, the top-layer thin films displayed degraded perpendicular properties. Then, it was proposed to use either a thin adhesion layer before the SiO_2 or another material like TiO_2 since it may have better adhesion properties to Co/Pd multilayers.

Fabrication Setup, Deposition and Characterization Co/Pd MLs thin films with an in-situ Applied In-plane Magnetic Field

Introduction

Magnetic materials have a preferred direction for magnetic moments within them which is referred to as the easy-axis (EA) of magnetization. For most crystalline thin films, this is induced along a preferred crystalline direction. For example, most conventional hard disk drives (HDDs) today use magnetic thin films to store binary information in the form magnetization alignment of nanograins on the surface of a disk. The EA of such recording media is pointed in the out-of-plane direction (perpendicular to the disk surface). This magnetization alignment is achieved by creating crystalline seed layers that cause the magnetic material to point its c-axis (hcp cell) in a perpendicular direction. If a magnetic field is applied in the in-plane direction with increasing magnitude, the magnetization will eventually align along this direction if the field is still applied, but with a relatively greater magnitude than is required to switch the magnetization along the perpendicular direction. This alignment causes the magnetization to align along the hard-axis (HA) of the media. Thus, an applied magnetic field in the out-of-plane (along the EA) direction will result in permanent switching of the magnetic domains within the material. However, when a magnetic field is applied in the in-plane direction (along the HA) the magnetization will be only temporarily rotated, and once turned off, the domains will randomize.

To advance perpendicular magnetic recording, a relatively magnetically-soft underlayer is applied below the recording layer, which is referred to as the soft-underlayer (SUL). This SUL is made to be either an amorphous or crystalline magnetic material with a preferred magnetization along the

in-plane direction. When an applied magnetic field from the recording head is generated, the SUL will mirror the writing pole and will produce a magnetic field across the bit area with greater magnitude than the pole alone. Soft magnetic materials have an EA and HA within the surface of the media, and it is important that these are established across the surface of the media to optimize the recording and reading of magnetic information.

It is possible to align the magnetization of materials in preferred directions using crystalline seed layers, an applied biasing field during material deposition at Curie temperatures, or by shaping the magnetic material with particular dimensions. To align the EA of soft magnetic materials, it is common to use a relatively weak magnetic field of a few Oe along the surface of the substrate. This ensures that each magnetic atom traveling towards the surface will experience a torque force that will align it in the preferred EA direction. On the other hand, not any studies have been performed to investigate relatively hard magnetic materials with biasing magnetic fields.

The research work below details the investigation of the effect of relatively large magnetic fields of ~2 kOe during the deposition of Co/Pd multilayered thin films. Since a Co/Pd multilayer is a candidate material for both conventional 2D and future 3D magnetic media, it was chosen for the analysis. Since the perpendicular alignment of such thin films is mainly occurs due to the surface properties of the Co and Pd bilayers, it is desirable to confirm whether a biasing field affects such compositions. A specially-designed sample holder was fabricated to produce a uniform and relatively high magnetic field in one in-plane direction along the sample surface. The figure 54 below shows the sample holder structure and location of the sample. Six permanent neodymium-based magnets were used to produce the desired magnetic field direction. The magnetic field was measured using a Hall-effect probe.

Experimental Setup

A reference Co/Pd multilayer thin film was fabricated without using a biasing field and was deposited on a glass substrate. Magnetic hysteresis curves were measured for this sample using the Faraday Effect,

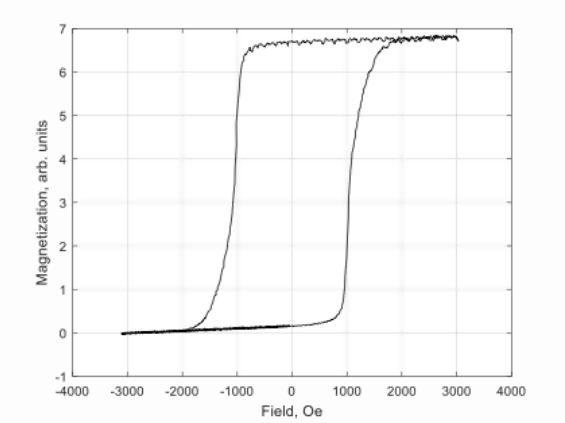

Figure 49 Reference sample of the Co/Pd

The rates for both Co and Pd were determined and optimized for the new holder using a biasing field. It was determined that the Pd rate and uniformity did not change using the new holder. Nevertheless, the rate and uniformity of the Co thin film was different than the one without an applied field. It was thus determined that the biasing filed may have some non-uniformity along the in-plane direction. For this investigation, the focus was on the center location of each sample and thus at the place of least differences for both deposition methods.

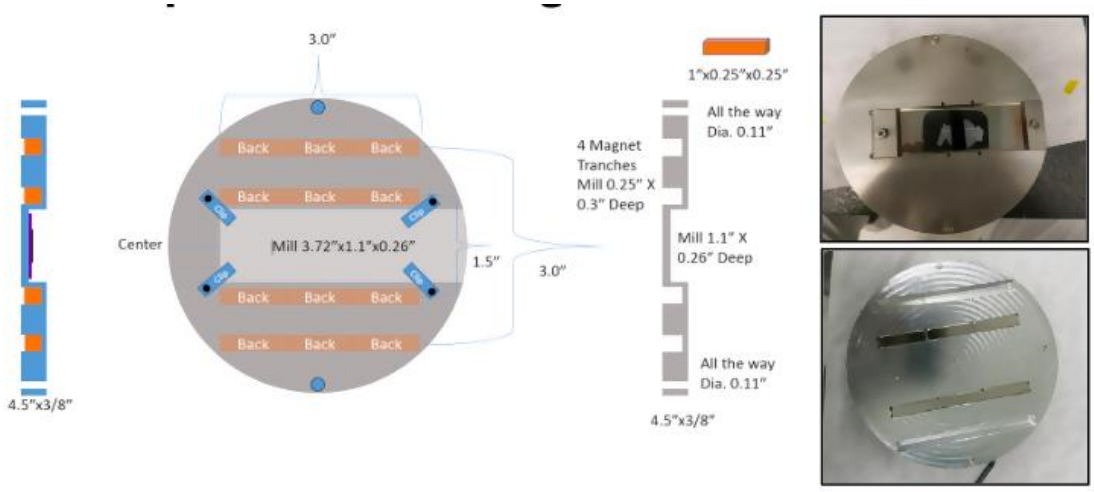

Figure 50 Design of the magnetic holder used to apply a bias field.

Material	Gas Flow	Processing Pressure	Target Source	Forward Power	Sample Height	Pre-Sputtering	Sputtering Time
Co	10 sccm	4.9 mTorr	DC 10%	75 W	21 mm	5 min	23 min
Pd	10 sccm	4.9 mTorr	DC 2.5%	19 W	21mm	5 min	20 min
SiO_2	10 sccm	4.9 mTorr	RF 100%	600 W	21mm	2 min	20 min

Table 2 Sputter process parameters and settings used to characterize optimal process

Results and Discussion

A Co/Pd thin film under a biasing magnetic field was fabricated and analyzed first with AFM/MFM and then with the Faraday Effect to determine its magnetic properties. Surprisingly, the MFM images indicated that the thin film was mostly magnetized in the up-direction which means that the

biasing magnetic field aligned the magnetization during deposition in the up-direction. The hysteresis curve appeared to have similar properties to the sample without an applied magnetic field.

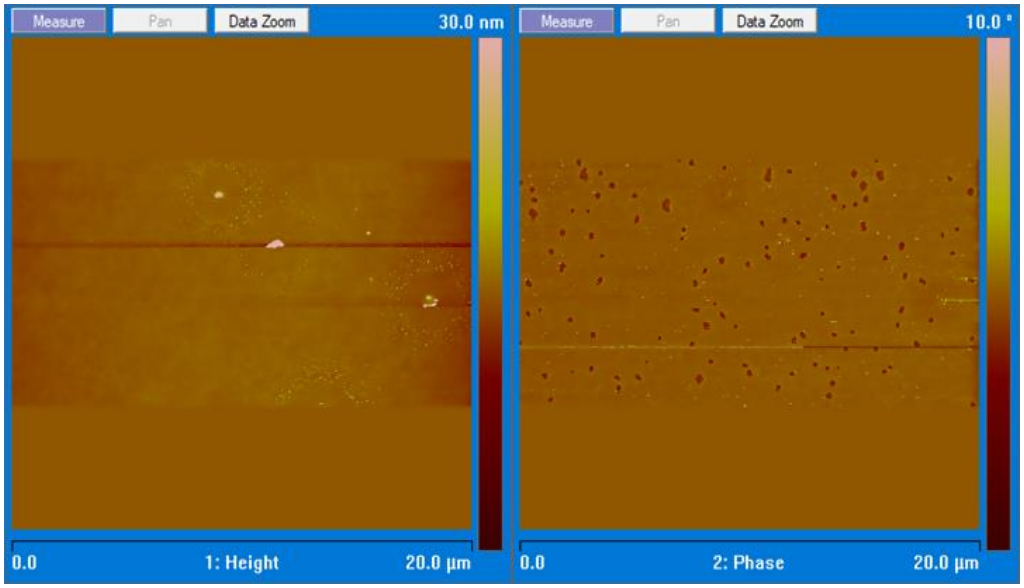

Figure 51 AFM image of the Co/Pd sample with a bias field which shows that some magnetic domains are pointed down.

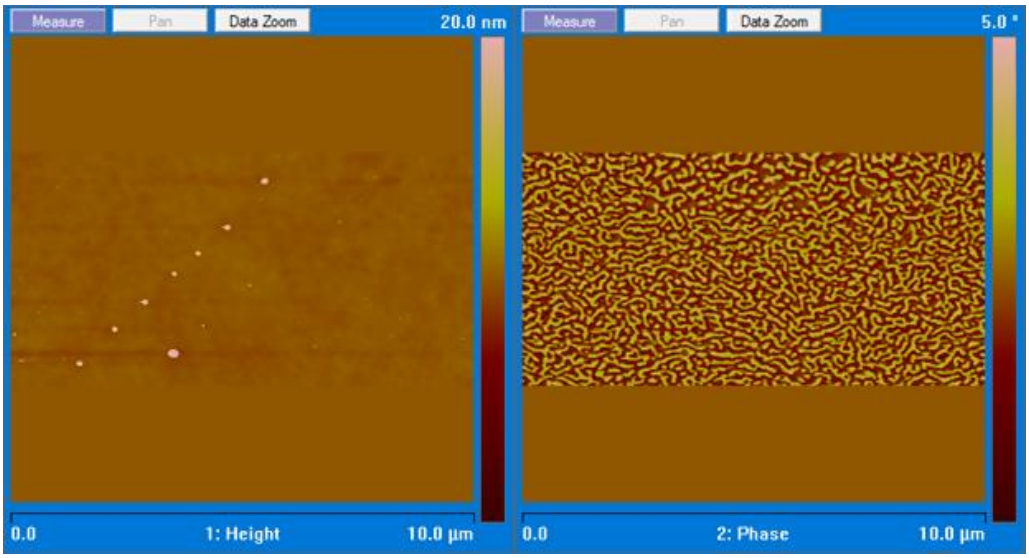

Figure 52 AFM images of the Co/Pd sample with no bias field applied.

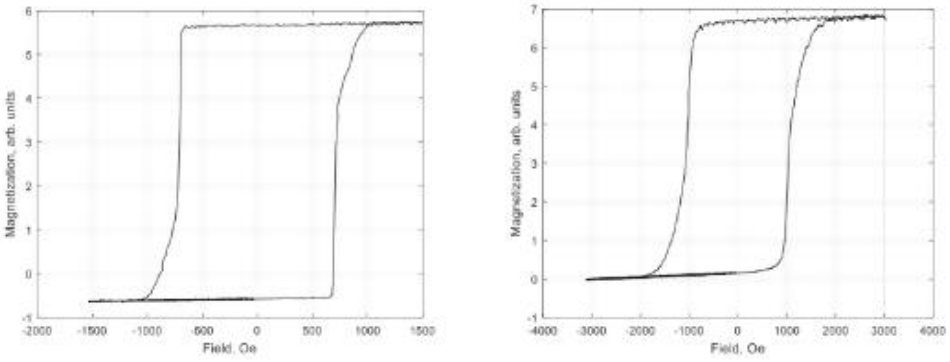

Figure 53 Applied bias hysteresis *vs* the non-bias hysteresis.

At this stage further investigation was conducted to determine if a preferred magnetization alignment direction was produced in the in-plane direction due to the applied biasing magnetic field. To perform this analysis, the Faraday Effect microscopy system was setup to produce alternating and decaying magnetic fields along the out-of-plane direction. A LabView program was constructed to monitor both applied magnetic fields while recording the magnetization state of the film being investigated. The system was further calibrated to produce a magnetic field near zero at the end of the "demagnetization" process. If the applied magnetic field had any noticeable effect on the in-plane magnetic properties of the Co/Pd thin film, "strip" domains would form across the entire media and align in the direction of the applied magnetic biasing field. On the other hand, if the media was not affected by the applied field, then commonly-generated fingerprint-like magnetic domains would form. To investigate this, the demagnetized sample was analyzed using magnetic force microscopy.

MFM images showed randomized magnetic domains which commonly appear for conventional Co/Pd ML media and thus showed that the biasing field did not have a noticeable effect on the media.

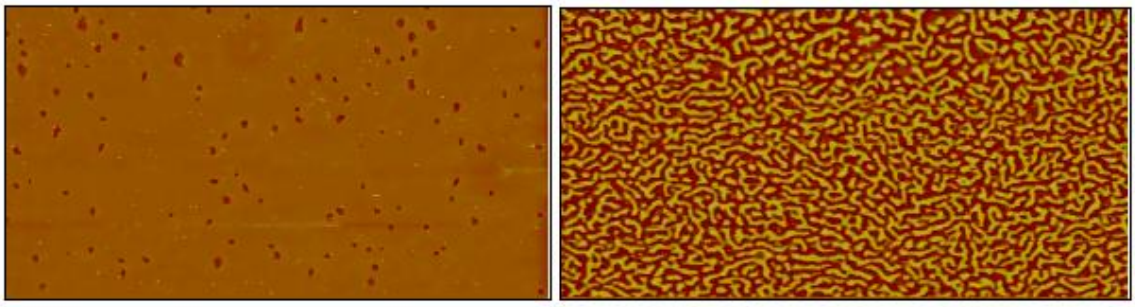

Figure 54 MFM images of the bias sample before and after it underwent a demagnetization process. The finger print area shows disordered magnetic domains.

To further confirm this finding, both samples were demagnetized and then the non-linear switching behavior of each thin film was recorded, starting from zero magnetization and increasing to a saturated magnetic field and then continuing to obtain a complete hysteresis curve. The results clearly show no significant differences between the two types of media. Some minor changes may be due to the slight non-uniformity of the Co bilayers for the applied biasing field sample.

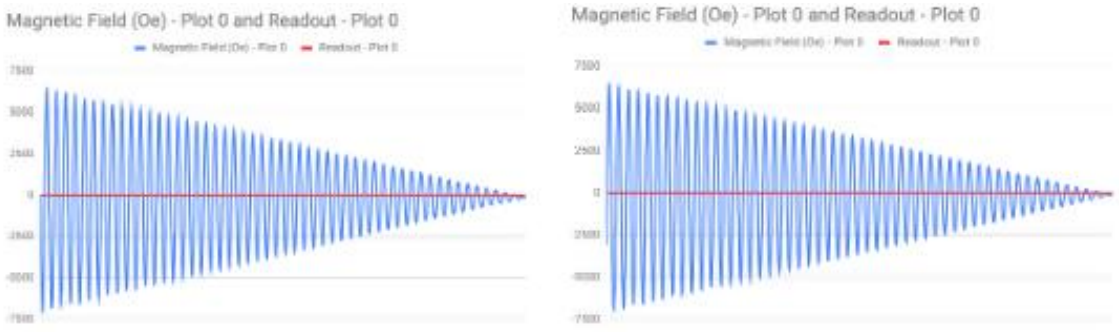

Figure 55 Figure confirming the magnetic field of the bias sample before and after demagnetization.

Conclusion

This investigation has confirmed that the MOKE with applied field and without an applied field MFM could be used to characterize the sputtering rates with an applied magnetic field. There are also media configurations that use both longitudinal and perpendicular 3D magnetic media. Finally, results show that Co/Pd ML media can be deposited with an in-plane biasing field for longitudinal media, thus making it a good candidate material for future recording media.

References

[1] G. O'Regan, "Gordon Moore," in *Giants of Computing*, 2013, pp. 197–200.

[2] Semiconductor Industry Association, *National technology roadmap for semiconductors*. 1997.

[3] C. A. Mack, "Fifty Years of Moore's Law," *IEEE Trans. Semicond. Manuf.*, vol. 24, no. 2, pp. 202–207, May 2011.

[4] S. E. Thompson and S. Parthasarathy, "Moore's law: the future of Si microelectronics," *Mater. Today*, vol. 9, no. 6, pp. 20–25, Jun. 2006.

[5] M. M. Waldrop, "The chips are down for Moore's law," *Nature*, vol. 530, no. 7589, pp. 144–147, Feb. 2016.

[6] M. M. Vopson, E. Zemaityte, M. Spreitzer, and E. Namvar, "Multiferroic composites for magnetic data storage beyond the super-paramagnetic limit," *J. Appl. Phys.*, vol. 116, no. 11, p. 113910, 2014.

[7] R. Ho, K. W. Mai, and M. A. Horowitz, "The future of wires," *Proc. IEEE*, vol. 89, no. 4, pp. 490–504, 2001.

[8] K. Liu, S. Sun, A. Majumdar, and V. J. Sorger, "Fundamental Scaling Laws in Nanophotonics," *Sci. Rep.*, vol. 6, p. 37419, Nov. 2016.

[9] "Website." [Online]. Available: https://www.researchgate.net/publication/281619688_Evolution_of_near_field_optical_microscopy. [Accessed: 31-Jan-2019].

[10] E. Betzig, A. Lewis, A. Harootunian, M. Isaacson, and E. Kratschmer, "Near Field Scanning Optical Microscopy (NSOM)," *Biophys. J.*, vol. 49, no. 1, pp. 269–279, Jan. 1986.

[11] D. M. Czajkowsky, J. Sun, and Z. Shao, "Illuminated up close: near-field optical microscopy of cell surfaces," *Nanomedicine*, vol. 11, no. 1, pp. 119–125, Jan. 2015.

[12] C. Manzo, T. S. van Zanten, and M. F. Garcia-Parajo, "Nanoscale fluorescence correlation spectroscopy on intact living cell membranes with NSOM probes," *Biophys. J.*, vol. 100, no. 2, pp. L8–10, Jan. 2011.

[13] G. Bourianoff, J. E. Brewer, R. Cavin, J. A. Hutchby, and V. Zhirnov, "Boolean Logic and Alternative Information-Processing Devices," *Computer* , vol. 41, no. 5, pp. 38–46, May 2008.

[14] M. Minsky, "Memoir on inventing the confocal scanning microscope," *Scanning*, vol. 10, no. 4, pp. 128–138, Aug. 1988.

[15] L. Novotny and B. Hecht, *Principles of Nano-Optics*. Cambridge University Press, 2012.

[16] S. Lal, S. Link, and N. J. Halas, "Nano-optics from sensing to waveguiding," *Nat. Photonics*, vol. 1, no. 11, pp. 641–648, Nov. 2007.

[17] S. W. Hell, "Increasing the Resolution of Far-Field Fluorescence Light Microscopy by Point-Spread-Function Engineering," in *Topics in Fluorescence Spectroscopy*, 2002, pp. 361–426.

[18] G. Lerosey, J. de Rosny, A. Tourin, and M. Fink, "Focusing beyond the diffraction limit with far-field time reversal," *Science*, vol. 315, no. 5815, pp. 1120–1122, Feb. 2007.

[19] A. Grbic, L. Jiang, and R. Merlin, "Near-Field Plates: Subdiffraction Focusing with Patterned Surfaces," *Science*, vol. 320, no. 5875, pp. 511–513, 2008.

[20] E. A. Ash and G. Nicholls, "Super-resolution Aperture Scanning Microscope," *Nature*, vol. 237, no. 5357, pp. 510–512, Jun. 1972.

[21] E. Betzig *et al.*, "Near-field magneto-optics and high density data storage," *Appl. Phys. Lett.*, vol. 61, no. 2, pp. 142–144, 1992.

[22] E. Betzig *et al.*, "Near-Field Magneto-Optics and High Density Storage," *Opt. Photonics News*, vol. 3, no. 12, p. 24, 1992.

[23] X. Zhang and Z. Liu, "Superlenses to overcome the diffraction limit," *Nat. Mater.*, vol. 7, no. 6, pp. 435–441, Jun. 2008.

[24] P. Hänninen, "Light microscopy: beyond the diffraction limit," *Nature*, vol. 419, no. 6909, p. 802, Oct. 2002.

[25] B. D. Terris, H. J. Mamin, D. Rugar, W. R. Studenmund, and G. S. Kino, "Near-field optical data storage using a solid immersion lens," *Appl. Phys. Lett.*, vol. 65, no. 4, pp. 388–390, Jul. 1994.

[26] M. Hausmann, B. Perner, A. Rapp, L. Wollweber, H. Scherthan, and K.-O. Greulich, "Near-field scanning optical microscopy in cell biology and cytogenetics," *Methods Mol. Biol.*, vol. 319, pp. 275–294, 2006.

[27] H. Volkmann, "Ernst abbe and his work," *Appl. Opt.*, vol. 5, no. 11, pp. 1720–1731, Nov. 1966.

[28] S. G. Lipson, H. Lipson, and D. S. Tannhauser, *Optical Physics*. Cambridge University Press, 1995.

[29] "Website." .

[30] S. Karimkashi, *Characteristics of Different Focusing Antennas in the Near Field Region*.

2011.

[31] B. Hecht *et al.*, “Scanning near-field optical microscopy with aperture probes: Fundamentals and applications,” *J. Chem. Phys.*, vol. 112, no. 18, pp. 7761–7774, 2000.

[32] C. M. Harris, “Product Review: Shedding Light on NSOM,” *Anal. Chem.*, vol. 75, no. 9, p. 223 A–228 A, 2003.

[33] K. Lieberman and A. Lewis, “Simultaneous scanning tunneling and optical near-field imaging with a micropipette,” *Appl. Phys. Lett.*, vol. 62, no. 12, pp. 1335–1337, 1993.

[34] G. C. Wetsel, R. H. Farahi, C. J. K. Richardson, and J. B. Spicer, “Approach interactions of scanned probes in dynamic pecking mode,” *Appl. Phys. Lett.*, vol. 79, no. 16, pp. 2657–2659, 2001.

[35] A. Rasmussen and V. Deckert, “New dimension in nano-imaging: breaking through the diffraction limit with scanning near-field optical microscopy,” *Anal. Bioanal. Chem.*, vol. 381, no. 1, pp. 165–172, Jan. 2005.

[36] Kramper, Kramper, Jebens, Muller, Mlynek, and Sandoghdar, “A novel fabrication method for fluorescence-based apertureless scanning near-field optical microscope probes,” *J. Microsc.*, vol. 194, no. 2–3, pp. 340–343, 1999.

[37] P. Kramper, A. Jebens, T. Müller, J. Mlynek, and V. Sandoghdar, “A novel fabrication method for fluorescence-based apertureless scanning near-field optical microscope probes,” *J. Microsc.*, vol. 194, no. Pt 2–3, pp. 340–343, May 1999.

[38] A. Tarun, M. R. H. Daza, N. Hayazawa, Y. Inouye, and S. Kawata, “Apertureless optical near-field fabrication using an atomic force microscope on photoresists,” *Appl. Phys. Lett.*, vol. 80, no. 18, pp. 3400–3402, 2002.

[39] A. Pack, W. Grill, and R. Wannemacher, “Apertureless near-field optical microscopy of metallic nanoparticles,” *Ultramicroscopy*, vol. 94, no. 2, pp. 109–123, 2003.

[40] W. Adams, M. Sadatgol, and D. Ö. Güney, “Review of near-field optics and superlenses for sub-diffraction-limited nano-imaging,” *AIP Adv.*, vol. 6, no. 10, p. 100701, Oct. 2016.

[41] L. Novotny, E. J. Sánchez, and X. Sunney Xie, “Near-field optical imaging using metal tips illuminated by higher-order Hermite–Gaussian beams,” *Ultramicroscopy*, vol. 71, no. 1–4, pp. 21–29, 1998.

[42] O. J. F. Martin and C. Girard, “Controlling and tuning strong optical field gradients at a local probe microscope tip apex,” *Appl. Phys. Lett.*, vol. 70, no. 6, pp. 705–707, 1997.

[43] E. J. Sánchez, L. Novotny, and X. Sunney Xie, “Near-Field Fluorescence Microscopy Based on Two-Photon Excitation with Metal Tips,” *Phys. Rev. Lett.*, vol. 82, no. 20, pp. 4014–4017,

1999.

[44] D. Haefliger, J. M. Plitzko, and R. Hillenbrand, “Contrast and scattering efficiency of scattering-type near-field optical probes,” *Appl. Phys. Lett.*, vol. 85, no. 19, p. 4466, 2004.

[45] D. W. Pohl, “Near Field Optics Seen as an Antenna Problem,” in *Near-Field Optics*, 2000, pp. 9–21.

[46] S. S. Choi, “Nanofabrication of Al-coated Oxide Aperture for NSOM Using Isotropic Etching Technique,” in *AIP Conference Proceedings*, 2003.

[47] S. S. Choi, M. S. Song, D. W. Kim, and M. J. Park, “Optimization procedures for metal-coated NSOM aperture array,” *Appl. Phys. A: Mater. Sci. Process.*, vol. 79, no. 4–6, pp. 1189–1193, 2004.

[48] E. Betzig, J. K. Trautman, T. D. Harris, J. S. Weiner, and R. L. Kostelak, “Breaking the Diffraction Barrier: Optical Microscopy on a Nanometric Scale,” *Science*, vol. 251, no. 5000, pp. 1468–1470, 1991.

[49] J. A. Veerman, A. M. Otter, L. Kuipers, and N. F. van Hulst, “High definition aperture probes for near-field optical microscopy fabricated by focused ion beam milling,” *Appl. Phys. Lett.*, vol. 72, no. 24, pp. 3115–3117, Jun. 1998.

[50] G. A. Valaskovic, M. Holton, and G. H. Morrison, “Parameter control, characterization, and optimization in the fabrication of optical fiber near-field probes,” *Appl. Opt.*, vol. 34, no. 7, p. 1215, 1995.

[51] L. Novotny, D. W. Pohl, and B. Hecht, “Scanning near-field optical probe with ultrasmall spot size,” *Opt. Lett.*, vol. 20, no. 9, p. 970, May 1995.

[52] Y. Sun *et al.*, “Growth and ferromagnetic resonance properties of nanometer-thick yttrium iron garnet films,” *Appl. Phys. Lett.*, vol. 101, no. 15, p. 152405, 2012.

[53] Y. Kajiwara *et al.*, “Transmission of electrical signals by spin-wave interconversion in a magnetic insulator,” *Nature*, vol. 464, no. 7286, pp. 262–266, 2010.

[54] J. Sone and S. Tsuji, *Intelligent Nanosystems for Energy, Information and Biological Technologies*. Springer, 2016.

[55] J. Xiao, G. E. W. Bauer, K.-C. Uchida, E. Saitoh, and S. Maekawa, “Erratum: Theory of magnon-driven spin Seebeck effect [Phys. Rev. B81, 214418 (2010)],” *Phys. Rev. B: Condens. Matter Mater. Phys.*, vol. 82, no. 9, 2010.

[56] R. L. Conger, “Nonlinear Damping Losses in YIG,” *J. Appl. Phys.*, vol. 32, no. 8, pp. 1525–1527, 1961.

[57] E. Montarroyos and S. M. Rezende, “Radiation damping of magnetostatic modes in yig,” *Solid State Commun.*, vol. 19, no. 8, pp. 795–798, 1976.

[58] C. L. Jermain *et al.*, “Increased low-temperature damping in yttrium iron garnet thin films,” *Phys. Rev. B Condens. Matter*, vol. 95, no. 17, p. 443, May 2017.

[59] P. B. Alers, “de Haas-van Alphen Oscillations in the Thermal and Electrical Magnetoresistance of Tin,” *Physical Review*, vol. 107, no. 4, pp. 959–960, 1957.

[60] B. Dieny, A. Granovsky, A. Vedyaev, N. Ryzhanova, C. Cowache, and L. G. Pereira, “Recent results on the giant magnetoresistance in magnetic multilayers (anisotropy, thermal variation and CCP-GMR),” *J. Magn. Magn. Mater.*, vol. 151, no. 3, pp. 378–387, 1995.

[61] B. Dieny, V. S. Speriosu, and S. Metin, “Thermal Variation of the Magnetoresistance of Soft Spin-Valve Multilayers,” *Europhys. Lett.*, vol. 15, no. 2, pp. 227–232, 1991.

[62] Eugene V. Nam and E. V. Nam, “Temperature dependence of yig films anisotropy,” in *IEEE International Magnetics Conference*, 1999.

[63] S. Hosseinzadeh *et al.*, “High saturation magnetization, low coercivity and fine YIG nanoparticles prepared by modifying co-precipitation method,” *J. Magn. Magn. Mater.*, vol. 476, pp. 355–360, 2019.

[64] R. L. White, “The physical boundaries to high-density magnetic recording,” *J. Magn. Magn. Mater.*, vol. 209, no. 1–3, pp. 1–5, 2000.

[65] Tu Chen, T. Chen, and R. Martin, “The physical limits of high density recording in metallic magnetic thin film media,” *IEEE Trans. Magn.*, vol. 15, no. 6, pp. 1444–1446, 1979.

[66] Hong Zhou, H. Zhou, and H. N. Bertram, “Micromagnetic study of longitudinal thin film media: effect of grain size distribution,” in *IEEE International Magnetics Conference*, 1999.

[67] G. A. Bertero *et al.*, “Longitudinal magnetic media designs for 60-200-Gb/in/sup 2/ recording,” *IEEE Trans. Magn.*, vol. 39, no. 2, pp. 651–656, 2003.

[68] S. Iwasaki, Y. Nakamura, and K. Ouchi, “Perpendicular magnetic recording with a composite anisotropy film,” *IEEE Trans. Magn.*, vol. 15, no. 6, pp. 1456–1458, 1979.

[69] M. Mallary, A. Torabi, and M. Benakli, “One terabit per square inch perpendicular recording conceptual design,” *IEEE Trans. Magn.*, vol. 38, no. 4, pp. 1719–1724, 2002.

[70] D. A. Thompson and D. A. Thompson, “THE ROLE OF PERPENDICULAR RECORDING IN THE FUTURE OF HARD DISK STORAGE,” *Journal of the Magnetics Society of Japan*, vol. 21, no. S_2_PMRC_97_2, pp. S2_9–15, 1997.

[71] D. Litvinov, M. H. Kryder, and S. Khizroev, “Recording physics of perpendicular media: hard

layers," *J. Magn. Magn. Mater.*, vol. 241, no. 2–3, pp. 453–465, 2002.

[72] M. Mikami, D. D. Djayaprawira, S. Yoshimura, and M. Takahashi, "Effect of oxidation process on grain-size reduction for longitudinal media using Ni-based amorphous seedlayer," *IEEE Trans. Magn.*, vol. 39, no. 5, pp. 2258–2260, 2003.

[73] Li-Lien Lee, L.-L. Lee, D. E. Laughlin, and D. N. Lambeth, "CrMn Underlayers for CoCrPt Thin Film Media," in *7th Joint MMM-Intermag Conference. Abstracts (Cat. No.98CH36275)*.

[74] R. E. Rottmayer *et al.*, "Heat-Assisted Magnetic Recording," *IEEE Trans. Magn.*, vol. 42, no. 10, pp. 2417–2421, Oct. 2006.

[75] M. H. Kryder *et al.*, "Heat Assisted Magnetic Recording," *Proc. IEEE*, vol. 96, no. 11, pp. 1810–1835, Nov. 2008.

[76] A. Ghoreyshi, S. Wang, and R. H. Victora, "Heat assisted magnetic recording media design using impedance modification method," in *2015 IEEE Magnetics Conference (INTERMAG)*, 2015.

[77] Yingfan Xu, J. P. Wang, C. K. Pock, Xiaomin Cheng, Z. S. Shan, and T. C. Chong, "Controlling the preferred orientation in granular CoCrPt:C thin films for high-areal density magnetic recording," *IEEE Trans. Magn.*, vol. 37, no. 4, pp. 1491–1493, Jul. 2001.

[78] M. Hirata *et al.*, "Integration of light delivery for heat assisted magnetic recording," in *2009 Asia-Pacific Magnetic Recording Conference*, 2009.

[79] T. Olson, M. Igarashi, B. Lengsfield, M. Shiimoto, M. Sugiyama, and R. Wood, "Detrimental Effects of the STO Vertical Field Component in MAMR," *IEEE Trans. Magn.*, vol. 51, no. 11, pp. 1–4, 2015.

[80] I. Tagawa, M. Shiimoto, M. Matsubara, S. Nosaki, Y. Urakami, and J. Aoyama, "Advantage of MAMR Read-Write Performance," *IEEE Trans. Magn.*, vol. 52, no. 9, pp. 1–4, 2016.